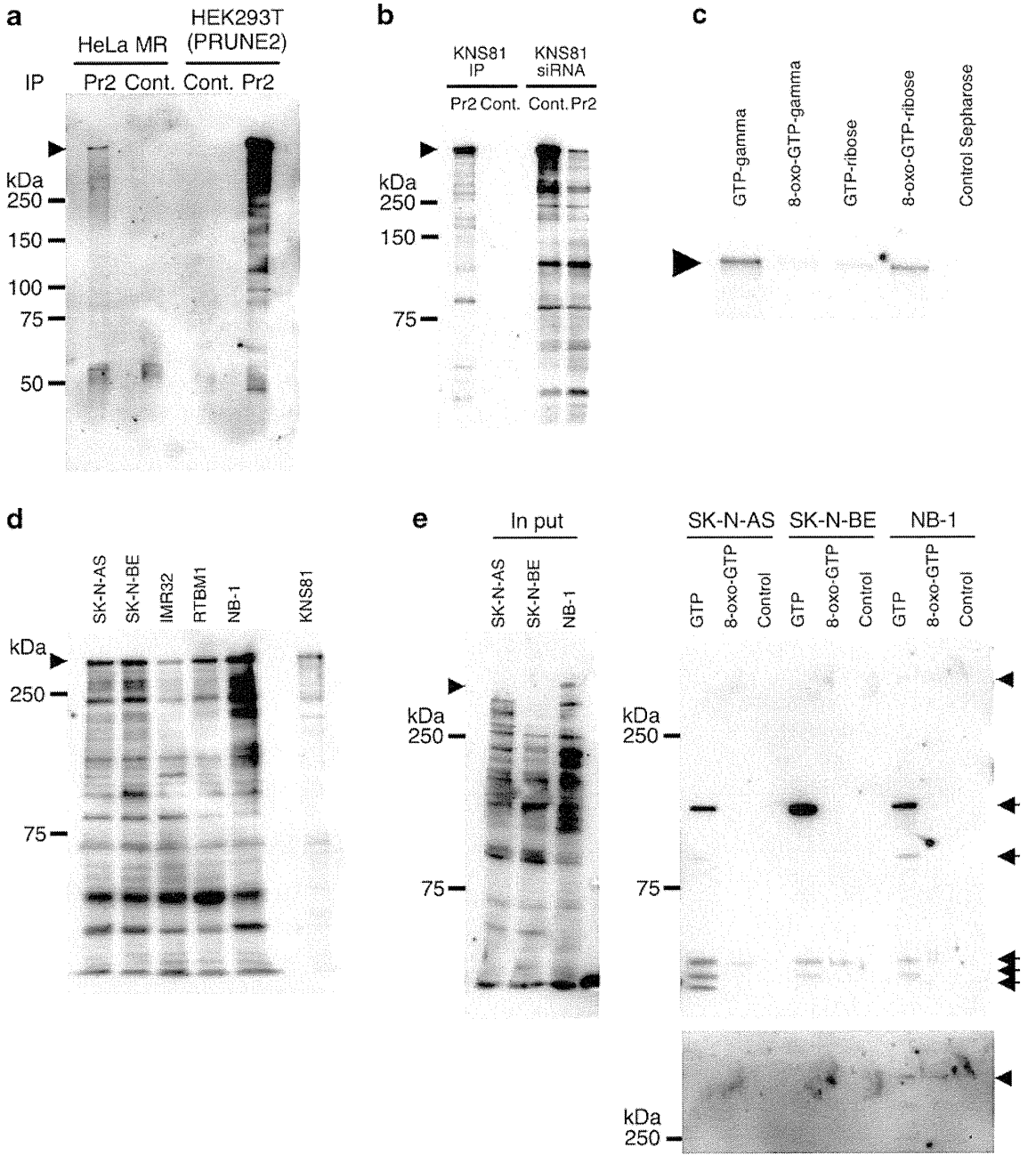

Fig. 4 Identification of endogenous PRUNE2 protein. **a** Western blot of samples precipitated with anti-hPr2N Ig (Pr2) or normal rabbit Ig (Cont.) from extracts prepared from HeLa MR or HEK293T cells transfected with pIRES2-EGFP:PRUNE2. The *arrowhead* indicates the signals for endogenous and recombinant full-length PRUNE2. **b** Confirmation of endogenous PRUNE2 protein by Western blot. In the *two right hand lanes*, extracts prepared from KNS81 cells treated with siRNA control (Cont.) or #04 (Pr2) were analyzed by Western blot with anti-hPr2N Ig. Samples precipitated from KNS81 extract with anti-hPr2N Ig (Pr2) or normal rabbit Ig (Cont.) were loaded on the *two left hand lanes*. The *arrowhead* indicates endogenous PRUNE2. **c** Interaction between PRUNE2 and 8-oxo-GTP. GTP and 8-oxo-GTP-immobilized-Sepharoses were incubated with a cytoplasmic extract prepared from KNS81 cells. Bound fractions from 33 μg of extract were analyzed by Western blot using anti-hPr2N Ig. The *arrowhead* indicates full-length PRUNE2 signals. **d** PRUNE2 proteins in whole cell extracts prepared from neuroblastoma cell lines. Ten micrograms of protein from whole cell extracts from each of the five neuroblastoma cell lines and KNS81 cells was subjected to Western blot using anti-Pr2N Ig. Bands corresponding to the full-length PRUNE2 are shown by an *arrowhead*. **e** Interaction between nucleotides and PRUNE2 protein derived from neuroblastoma cell lines. Cytoplasmic extracts prepared from SK-N-AS, SK-N-BE, and NB-1 were subjected to a pull-down assay with ribose linked GTP- or 8-oxo-GTP-immobilized Sepharose. The bound fractions from 167 μg of protein of each extract (*right*) and 10 μg of protein of each input extract (*left*) were analyzed by Western blot with anti-Pr2N Ig. An *arrowhead* indicates full-length PRUNE2 proteins, and *arrows* indicate short forms of PRUNE2 in the bound fractions. Bands corresponding to the full-length PRUNE2 protein shown with an *arrowhead* were clear in an image with longer exposure (*right bottom*)

Table 1 Proteins co-immunoprecipitated with anti-PRUNE2 antibody but not with control Ig

Protein name	Accession number	Mascot score
Multifunctional protein ADE2	NP_001072993	107
Membrane-associated progesterone receptor component 1	NP_006658	68
B-cell receptor-associated protein 31	P51572	62
Chondroitin sulfate synthase 1	NP_055733	54
Diablo	NP_063940	53
Occludin	NP_002529	46
Ubiquitin carboxyl-terminal hydrolase 17-like protein	Q7RTZ2	45
NADH-ubiquinone oxidoreductase 75 kDa subunit, mitochondrial precursor	NP_004997	44
Synaptotagmin-like protein 4	Q96C24	43
DNA polymerase mu	NP_037416	43
Antigen KI-67	P46013	41
Malate dehydrogenase, mitochondrial precursor	NP_005909	41
POLM protein	AAH49202	41
Isoform B of LIM/homeobox protein Lhx6.1	NP_954629	40
Insulin-like growth factor binding protein-like 1	CAD13245	40
Hypothetical protein LOC283461	NP_001026918	40
Neutral alpha-glucosidase AB	Q14697	40
Forkhead box P1 isoform 2	NP_001012523	40
Hornerin	NP_001009931	40
T-cell activation Rho GTPase-activating protein	NP_473455	39

PRUNE2 Is Highly Expressed in Adult DRG Neurons

We performed quantitative real time RT-PCR of *PRUNE2* mRNA using total RNA from human tissues and two sets of primers, RT900 (exon 7) and RT7500 (exon 8/9) (Fig. 5a). The highest expression of *PRUNE2* mRNA was detected in total RNA from DRG tissues. Whole brain, spinal cord, uterus, and prostate also expressed high levels of *PRUNE2* mRNA. Thus, *PRUNE2* expression was relatively high in human adult nerve tissues, although it was very low in fetal brain.

To examine the age-dependent expression of *Prune2* mRNA, we analyzed the expression level of *Prune2* mRNA in nerve tissues (cortex, cerebellum, brain stem, and spinal cord) prepared from C57BL/6J mice at 3 and 11 days, 3, 6, 11, and 52 weeks of age. The results showed that *Prune2* expression is highest in the spinal cord and, to a lesser extent, in the brain stem in all ages examined and that expression is elevated considerably from 11 days to 3 weeks after birth (Fig. 5b). As observed for human *PRUNE2*, the expression level of *Prune2* mRNA in the DRG was two times higher than that in the spinal cord at 11 weeks of age (Fig. 5c).

To identify cells expressing PRUNE2 protein in the human DRG, we performed immunohistochemistry using anti-hPr2N Ig. As shown in Fig. 6a, DRG neurons exhibit the strongest immunoreactivity in their soma and to a lesser extent in satellite and Schwann cells.

Discussion

Using nucleotide-immobilized-Sepharose, mouse and human PRUNE2 were identified as 8-oxo-GTP/GTP-associated proteins. Soh et al. reported that BNIPXL, which corresponds to the C-terminal region of PRUNE2, interacts with RhoA and RhoC (Soh and Low 2008). Therefore, it is likely that PRUNE2 protein, which is associated with the Rho family small G proteins and may indirectly bind to 8-oxo-GTP/GTP-immobilized-Sepharose, was detected in the nucleotide-bound fractions. The N-terminal region of PRUNE2 has homology with PRUNE, a DHH (Asp-His-His) super family protein (D'Angelo et al. 2004). Several enzymes of the DHH family including exopolyphosphatase of budding yeast (*Sc*PPX) possess phosphohydrolase activity (Wurst and Kornberg 1994). Recently, PRUNE was reported to have exopolyphosphatase activity against adenosine 5′-tetraphosphate (Tammenkoski et al. 2008). Thus, PRUNE2 may recognize the phosphate group of 8-oxo-GTP/GTP. PRUNE2 protein is expressed in normal tissues, such as DRG neurons, and in malignant tissues. In our results, KNS81 and HeLa MR expressed full-length PRUNE2 as major products. By contrast, the full-length protein is a relatively minor product in neuroblastoma cell lines, such as NB-1, SK-N-AS, SK-N-BE, RTBM1, and IMR32 cells. PRUNE2 proteins with different molecular

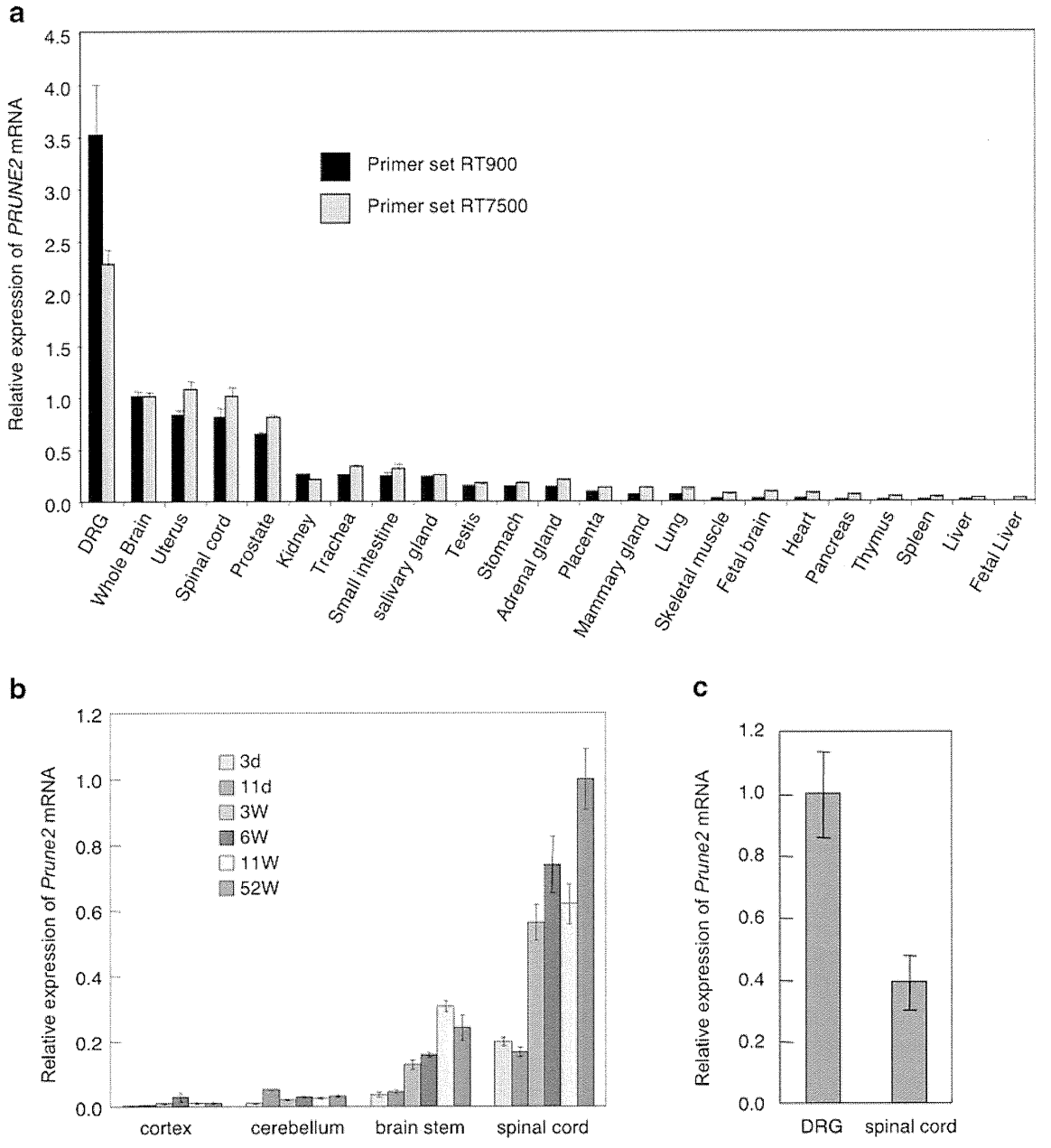

Fig. 5 Expression of *PRUNE2* in tissues. **a** *PRUNE2* mRNA levels in human tissues were analyzed by quantitative real time RT-PCR using two primer sets, RT900 and RT7500. **b** *PRUNE2* mRNA levels in nerve tissues of mice at different weeks of age were analyzed by quantitative real time RT-PCR. **c** *PRUNE2* mRNA levels in the spinal cord and DRG of 11-week-old mice were compared. The levels of relative expression are expressed as the mean ± SD of three measurements

sizes might have different properties or functions in different tissues and/or different cells, especially with regard to its association with GTP and/or 8-oxo-GTP. Oxidation of GTP occurs under oxidative stress, which is known to be much higher in malignant tissues than in normal tissues. The results suggest that higher levels of 8-oxo-GTP present in malignant tissues might alter the function of various variant PRUNE2 proteins, thereby contributing to the malignancy.

Machida et al. suggested that the pro-apoptotic function of BMCC1 is important for determining the fate of neuroblastoma (Machida et al. 2006). In this report, we observed that *PRUNE2* is constitutively expressed in adult nerve tissue and the prostate, suggesting that PRUNE2 may have a physiological role in these tissues, in addition to promoting apoptosis in neuroblastoma. KNS81, a cell line derived from glioblastoma, exhibited relatively high levels of *PRUNE2* expres-

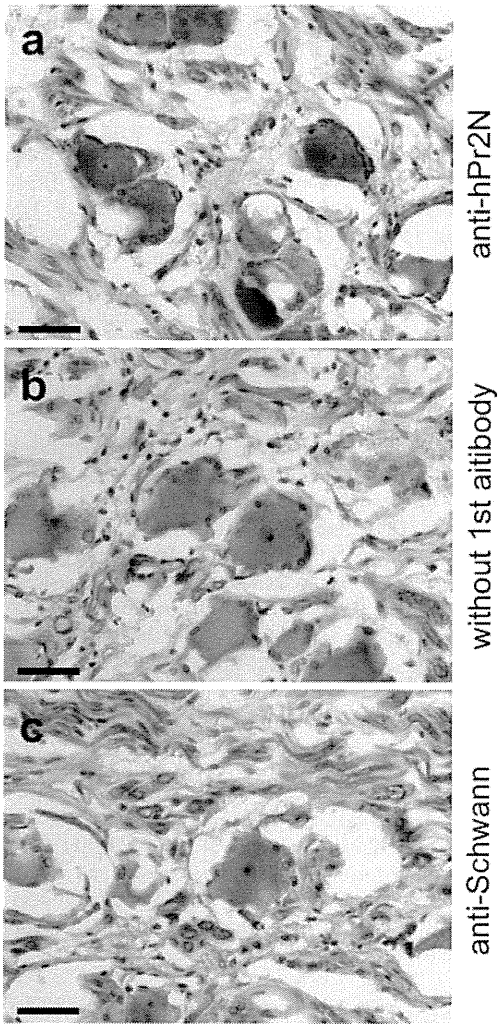

Fig. 6 PRUNE2 protein in human DRG neurons. **a** Immunohistochemical detection of PRUNE2. Frozen sections of human DRG were prepared and reacted with anti-hPr2N Ig as described in "Materials and Methods". **b** Frozen sections were processed for the immunohistochemistry in the absence of the primary anti-hPr2N Ig. **c** Frozen sections were reacted with anti-Schwann Ig. *Scale bars*=50 μm

sion compared with that in HeLa MR and SH-SY5Y. *PRUNE2* may be expressed and function in glial cells such as astrocytes in the central nervous system, in addition to DRG neurons in the peripheral nervous system. From KNS81 cells, we identified 20 candidates for PRUNE2-associating proteins by co-immunoprecipitation. Among them, T-cell activation Rho GTPase-activating protein, TAGAP, is one of the most interesting molecules because the C-terminus of PRUNE2 was previously reported to inactivate Rho family small G protein by inhibiting a RhoGEF, Lbc (Soh and Low 2008). As TAGAP possesses a Rho-GAP domain (Mao et al. 2004), PRUNE2 might regulate the activity of Rho family small G proteins by controlling the function of TAGAP in addition to Lbc. In addition to TAGAP, Smac/DIABLO was also identified in the complex. Smac/DIABLO enhances apoptosis by inhibiting inhibitors of apoptosis proteins (Martinez-Ruiz et al. 2008), and its expression was observed in the peripheral nervous system (Perrelet et al. 2004). It is likely that PRUNE2/BMCC1 regulates apoptosis through an interaction with Smac/DIABLO.

Recently, BMCC1 was reported to be up-regulated in prostate cancer (Clarke et al. 2009). However, other groups reported conflicting data (Lavin et al. 2009). Moreover, Price et al. found that the expression levels of *C9orf65*, which corresponds to the 5′-terminal region of *PRUNE2*, was high in LMS, but low in GIST (Price et al. 2007). Adversely, they showed that the levels of *OBSCN* mRNA were low in LMS, but high in GIST. The BCH domain in the C-terminal region of PRUNE2 has been reported to inhibit RhoA and cellular transformation mediated by Lbc RhoGEF (Soh and Low 2008). On the other hand, OBSCN protein was reported to possess RhoGEF activity and to activate RhoA (Bowman et al. 2008; Ford-Speelman et al. 2009). It is possible that PRUNE2 and OBSCN may competitively regulate RhoA activity, thus contributing to the characteristics of LMS and GIST cells. Because strong activation of RhoA was reported to induce growth cone collapse and neurite retraction (Jalink et al. 1994), the elevated expression of *PRUNE2* in adult nerve tissues may contribute to the maintenance of mature neural networks, although we do not have any direct evidence.

For future studies of the physiological function of PRUNE2 in vitro, three neuroblastoma-derived cell lines, SK-N-AS, SK-N-BE, and NB-1 may be useful because PRUNE2 is highly expressed in the mature nervous system. In vivo analysis using genetically modified mice may be helpful in understanding the function of PRUNE2. It was reported that portions of the *PRUNE2* gene are likely to be expressed in short forms (Jalink et al. 1994). It is possible that BMCC1 or BNIPXL is a short variant of *PRUNE2* gene products. However, there is no paper reporting the biochemical and physiological functions of full-length PRUNE2. More detailed analyses are necessary to understand the biological significance of full-length PRUNE2 and its variants.

In the present study, we isolated the full-length *PRUNE2* cDNA and demonstrated the full-length PRUNE2 protein in HeLa MR and KNS81 cells. These data indicate that the two malignant tumor-associated genes, *C9orf65* and *BMCC1/BNIPXL*, are transcribed as a single mRNA, *PRUNE2* mRNA, which is translated to a large PRUNE2 protein. The nerve tissue-specific and post-development expression of *PRUNE2/Prune2* suggests that PRUNE2 may contribute to the maintenance of mature nervous systems.

Acknowledgments We thank Dr. Toru Iwaki for providing human tissue samples and helpful discussion. We thank Dr. Masaki Matsumoto from the Division of Proteomics of the Medical Institute of Bioregulation for helpful discussions. We thank Mizuho Oda, Emiko Koba, and Masumi Ohtsu from the Laboratory for Technical Support of the Medical Institute of Bioregulation and Setsuko Kitamura and Kazumi Asakawa for their technical assistance. This work was supported by MEXT KAKENHI 20013034, 21117512, JSPS KAKENHI 19390114, and by the Kyushu University Global COE program. T.I. is a research fellow of JSPS.

References

Altschul SF, Gish W, Miller W, Myers EW, Lipman DJ (1990) Basic local alignment search tool. J Mol Biol 215:403–410

Biedler JL, Helson L, Spengler BA (1973) Morphology and growth, tumorigenicity, and cytogenetics of human neuroblastoma cells in continuous culture. Cancer Res 33:2643–2652

Bowman AL, Catino DH, Strong JC, Randall WR, Kontrogianni-Konstantopoulos A, Bloch RJ (2008) The rho-guanine nucleotide exchange factor domain of obscurin regulates assembly of titin at the Z-disk through interactions with Ran binding protein 9. Mol Biol Cell 19:3782–3792

Clarke RA, Zhao Z, Guo AY et al (2009) New genomic structure for prostate cancer specific gene PCA3 within BMCC1: implications for prostate cancer detection and progression. PLoS ONE 4:e4995

D'Angelo A, Garzia L, Andre A et al (2004) Prune cAMP phosphodiesterase binds nm23-H1 and promotes cancer metastasis. Cancer Cell 5:137–149

Ford-Speelman DL, Roche JA, Bowman AL, Bloch RJ (2009) The rho-guanine nucleotide exchange factor domain of obscurin activates rhoA signaling in skeletal muscle. Mol Biol Cell 20:3905–3917

Iida T, Furuta A, Nakabeppu Y, Iwaki T (2004) Defense mechanism to oxidative DNA damage in glial cells. Neuropathology 24:125–130

Jalink K, van Corven EJ, Hengeveld T, Morii N, Narumiya S, Moolenaar WH (1994) Inhibition of lysophosphatidate- and thrombin-induced neurite retraction and neuronal cell rounding by ADP ribosylation of the small GTP-binding protein Rho. J Cell Biol 126:801–810

Kajitani K, Yamaguchi H, Dan Y, Furuichi M, Kang D, Nakabeppu Y (2006) MTH1, an oxidized purine nucleoside triphosphatase, suppresses the accumulation of oxidative damage of nucleic acids in the hippocampal microglia during kainate-induced excitotoxicity. J Neurosci 26:1688–1698

Larkin MA, Blackshields G, Brown NP et al (2007) Clustal W and Clustal X version 2.0. Bioinformatics 23:2947–2948

Lavin MF, Clarke R, Gardiner RA (2009) Differential expression of PCA3 and BMCC1 in prostate cancer. Prostate 69:1713–1714, author reply 1715

Machida T, Fujita T, Ooo ML et al (2006) Increased expression of proapoptotic BMCC1, a novel gene with the BNIP2 and Cdc42GAP homology (BCH) domain, is associated with favorable prognosis in human neuroblastomas. Oncogene 25:1931–1942

Mao M, Biery MC, Kobayashi SV et al (2004) T lymphocyte activation gene identification by coregulated expression on DNA microarrays. Genomics 83:989–999

Martinez-Ruiz G, Maldonado V, Ceballos-Cancino G, Grajeda JP, Melendez-Zajgla J (2008) Role of Smac/DIABLO in cancer progression. J Exp Clin Cancer Res 27:48

Nakabeppu Y, Nathans D (1991) A naturally occurring truncated form of FosB that inhibits Fos/Jun transcriptional activity. Cell 64:751–759

Nakabeppu Y, Kajitani K, Sakamoto K, Yamaguchi H, Tsuchimoto D (2006a) MTH1, an oxidized purine nucleoside triphosphatase, prevents the cytotoxicity and neurotoxicity of oxidized purine nucleotides. DNA Repair (Amst) 5:761–772

Nakabeppu Y, Sakumi K, Sakamoto K, Tsuchimoto D, Tsuzuki T, Nakatsu Y (2006b) Mutagenesis and carcinogenesis caused by the oxidation of nucleic acids. Biol Chem 387:373–379

Nonaka M, Tsuchimoto D, Sakumi K, Nakabeppu Y (2009) Mouse RS21-C6 is a mammalian 2′-deoxycytidine 5′-triphosphate pyrophosphohydrolase that prefers 5-iodocytosine. FEBS J 276:1654–1666

Perrelet D, Perrin FE, Liston P et al (2004) Motoneuron resistance to apoptotic cell death in vivo correlates with the ratio between X-linked inhibitor of apoptosis proteins (XIAPs) and its inhibitor, XIAP-associated factor 1. J Neurosci 24:3777–3785

Price ND, Trent J, El-Naggar AK et al (2007) Highly accurate two-gene classifier for differentiating gastrointestinal stromal tumors and leiomyosarcomas. Proc Natl Acad Sci USA 104:3414–3419

Soh UJ, Low BC (2008) BNIP2 extra long inhibits RhoA and cellular transformation by Lbc RhoGEF via its BCH domain. J Cell Sci 121:1739–1749

Tammenkoski M, Koivula K, Cusanelli E et al (2008) Human metastasis regulator protein H-prune is a short-chain exopolyphosphatase. Biochemistry 47:9707–9713

Torisu K, Tsuchimoto D, Ohnishi Y, Nakabeppu Y (2005) Hematopoietic tissue-specific expression of mouse Neil3 for endonuclease VIII-like protein. J Biochem 138:763–772

Tsuchimoto D, Sakai Y, Sakumi K et al (2001) Human APE2 protein is mostly localized in the nuclei and to some extent in the mitochondria, while nuclear APE2 is partly associated with proliferating cell nuclear antigen. Nucleic Acids Res 29:2349–2360

Wurst H, Kornberg A (1994) A soluble exopolyphosphatase of *Saccharomyces cerevisiae*. Purification and characterization. J Biol Chem 269:10996–11001

SAGE-Hindawi Access to Research
Parkinson's Disease
Volume 2011, Article ID 307875, 9 pages
doi:10.4061/2011/307875

Review Article

Therapeutic Effects of Hydrogen in Animal Models of Parkinson's Disease

Kyota Fujita,[1] Yusaku Nakabeppu,[2] and Mami Noda[1]

[1] *Laboratory of Pathophysiology, Graduate School of Pharmaceutical Sciences, Kyushu University, 3-1-1 Maidashi, Fukuoka 812-8582, Japan*
[2] *Division of Neurofunctional Genomics, Medical Institute of Bioregulation, Kyushu University, Fukuoka 812-8582, Japan*

Correspondence should be addressed to Mami Noda, noda@phar.kyushu-u.ac.jp

Received 15 September 2010; Revised 5 January 2011; Accepted 14 March 2011

Academic Editor: David S. Park

Since the first description of Parkinson's disease (PD) nearly two centuries ago, a number of studies have revealed the clinical symptoms, pathology, and therapeutic approaches to overcome this intractable neurodegenerative disease. 1-methy-4-phenyl-1,2,3,6-tetrahydropyridine (MPTP) and 6-hydroxydopamine (6-OHDA) are neurotoxins which produce Parkinsonian pathology. From the animal studies using these neurotoxins, it has become well established that oxidative stress is a primary cause of, and essential for, cellular apoptosis in dopaminergic neurons. Here, we describe the mechanism whereby oxidative stress evokes irreversible cell death, and propose a novel therapeutic strategy for PD using molecular hydrogen. Hydrogen has an ability to reduce oxidative damage and ameliorate the loss of nigrostriatal dopaminergic neuronal pathway in two experimental animal models. Thus, it is strongly suggested that hydrogen might provide a great advantage to prevent or minimize the onset and progression of PD.

1. Introduction

The central pathological feature of PD was loss of neurons in substantia nigra pars compacta (SNpc). DA depletion by the loss of dopaminergic neurons in SNpc is a primary symptom of PD [1]. PD is one of the most common neurodegenerative and progressive diseases, along with Alzheimer's disease (AD) [2, 3]. In these last two decades, many lines of evidence have emerged to suggest that oxidative stress is closely related to the onset and the progression of PD and AD.

Using neurotoxins in experimental animal models, an enormous number of studies have been undertaken to develop neuroprotective drugs against PD. MPTP (1-methyl-4-phenyl-1,2,3,6-tetrahydropyridine) was found to be a by-product of the chemical synthesis of a meperidine analog with potent heroin-like effects [4, 5]. MPTP has the ability to induce PD-like pathology and has been used in various species including nonhuman primates, and rodents. Among the neurotoxic mechanism of MPTP, mitochondrial impairment is highly associated with oxidative damage and related neurodegeneration; the detailed mechanism and the linkage between oxidative damage and neurodegeneration are discussed in this review. Although MPTP-induced PD model animals are regarded as the best reproducible model, another neurotoxin, 6-hydroxydopamine (6-OHDA; 2,4,5-trihydroxyphenylethylamine), is also used for toxin-induced animal model of PD [6].

Many trials have focused on the reduction of oxidative stress as a therapeutic strategy because oxidative stress is regarded as one of the major risk factors in the onset of PD as mentioned above. However, there are still no known antioxidant drugs which are clinically used to prevent PD. Here, the neurotoxic mechanism of MPTP which induces Parkinsonian pathology and behavior, and how molecular hydrogen prevents them, is discussed in this review.

2. Acute and Chronic PD Model Induced by MPTP

MPTP is a protoxin which is high lipophilic molecule, and can penetrate the blood-brain barrier (BBB) after systemic administration. After crossing the BBB, MPTP is readily

converted to 1-methyl-4-phenylpyridinium ion (MPP^+), an actual toxin which can lead to dopaminergic neurodegeneration [7]. MPTP conversion to MPP^+ is dependent on the activity of monoamine oxidase B (MAO-B) by a two-step reaction. First, MPTP is converted to the intermediate 1-methyl-4-phenyl-2,3-dihydropyridinium ($MPDP^+$), catalyzed by MAO-B [8]. Then, unstable $MPDP^+$ dissociates to MPP^+ and MPTP [9, 10]. Conversion of MPTP to $MPDP^+$ occurs in glial cells and serotonergic cells, not in dopaminergic cells. Dopaminergic neurons exhibit a high-affinity uptake process of MPP^+ through the dopamine transporter, which allows the neurotoxin MPP^+ to cause selective dopaminergic neuronal loss [11]. Inside the neurons, MPP^+ accumulates in the mitochondrial matrix, whose uptake is driven by mitochondrial transmembrane potential gradient [12, 13]. MPP^+ impairs mitochondrial respiration by inhibiting the multisubunit enzyme complex I of the mitochondrial electron transport chain [14, 15]. Inhibition of complex I causes two early and major events: ATP depletion and the buildup of reactive oxygen species (ROS). Complex I activity appears to be decreased by more than 50% to induce nonsynaptic mitochondrial ATP depletion. *In vitro* studies also revealed that mitochondria which are isolated from whole brain require 70% inhibition of complex I activity for ATP depletion. However, *in vivo* MPTP administration causes only a transient 20% reduction of ATP levels in mouse striatum and midbrain [16]. *In vitro* experiments with synaptic mitochondria show that exceeding a threshold of 25% inhibition of complex I results in significant ATP depletion [17]. These findings may imply that synaptic mitochondria show a better correlation with both complex I inhibition and ATP depletion than those in somatic mitochondria. This may answer the question why dopaminergic neurodegeneration shows retrograde degeneration from striatal nerve terminals, which are rich in synaptic mitochondria.

The extents of loss of dopaminergic neurons and behavioral alteration vary depending on differences in the protocol of MPTP administration. Acute administration (20 mg/kg, 3 or 4 times at 2 hours interval) can reduce ~70% of nigral dopaminergic neurons and ~90% of striatal nerve terminal fibers 7 days after administration when the loss of nigral neurons is stable [18] (see Table 1). Up to 10% of MPTP-administered involuntarily die within 24 hours because of cardiovascular side effects, not of dopaminergic neuronal loss, and mice were immobilized until 24 to 48 hours. Striatal MPP^+ level was increased and peaked ~3 hours after the last administration of MPTP. In subacute injection model, MPTP is administrated once a day at 30 mg/kg for 5 consecutive days. Since mild doses of MPTP was administered compared to the acute injection model, an incidence of death was lower in the subacute injection model. Loss of nigral dopaminergic neurons and striatal nerve terminal fibers was also less than acute injection model; ~50% loss of fibers and ~40% loss of nigral dopaminergic neurons were observed 3 weeks after the last day of MPTP administration. For the continuous administration model, MPTP was infused subcutaneously (s.c.) or intraperitoneally (i.p) using osmotic pumps. Our observation revealed that subcutaneous infusion of MPTP at 45 mg/kg/day for 28 days caused 50% loss of nigral dopaminergic neurons [19]. Continuous administration of MPTP subacutely or chronically caused less dopaminergic neuronal loss, which might reflect sprouting of residual fibers or *de novo* appearance of tyrosine hydroxylase-(TH-) positive dopaminergic neurons in DA-depleted striatum [22–25]. Therefore, chronic recovery and damage of TH fiber may occur simultaneously in nigrostriatal pathway.

The chronic administration model had several unique features which were regarded as better phenomena as PD model: (i) formation of inclusion bodies which were positive for alpha-synuclein and ubiquitin, (ii) loss of noradrenergic (NE) neurons in locus coeruleus, (iii) impairment of ubiquitin-proteasome system, and (iv) behavioral alteration. Especially, loss of NE neurons was observed as in human PD [26], and dopamine β-hydroxylase knockout ($Dbh^{-/-}$) mice which lack NE neurons showed more profound motor deficit compared to MPTP-treated mice [27]. Furthermore, bolus administration of MPTP did not induce inclusion bodies formation [21]. Therefore, chronic administration model using an osmotic pump could mimic human PD feature.

3. Oxidative Damage and Apoptotic Signals in MPTP Model

ROS, mostly a superoxide, is produced in mitochondria because of a leak of electrons from the respiratory chain inhibited by MPP^+ [28]. Energy metabolic inhibition and ROS overproduction have their peak several hours after MPTP administration, which trigger the downstream of cellular apoptosis and neurodegeneration days after MPTP treatment [29, 30]. In PD patients, iron level is increased selectively in SNpc, which leads to the greater accessibility of ferrous iron (Fe^{2+}) with hydrogen peroxide and thus generating hydroxyl radical (•OH) [31]. Moreover, lipid peroxidation, protein carbonyls, and 8-oxo-7,8-dihydroguanine (8-oxoG) are increased, which means that cellular lipids, proteins, and DNA are highly exposed to oxidative stress [32, 33]. Such oxidative damage occurs prior to the cellular apoptosis processes.

Sources of ROS are various, and ROS is produced not only in neurons but also in glial cells such as microglia when they become activated (reactive) and show morphological changes [34]. From dopaminergic neurons, superoxide is produced not only in mitochondria but also by auto-oxidation of DA [35]. It is known that auto-oxidation of DA leads to the production of DA (semi)quinones that are converted into aminochrome, which can generate superoxide [36, 37]. Increased ROS causes oxidative damage to DNA [38, 39], cellular lipid peroxidation [40, 41], and stress-related signaling activation such as MAPK and JNK activation [42–44].

Oxidative stress in DNA leads to cellular apoptosis which is mediated by p53 activation and p53-derived Bax translocation to mitochondria. Furthermore, Bax translocation and cytochrome c from mitochondria to the cytosol leads to caspase-dependent apoptosis [45]. Oxidative damage in DNA induces not only caspase-dependent apoptosis but also caspase-independent apoptosis. Among the five normal

Table 1: Comparison of representative MPTP-PD models. Each written model is representative and reproducible examples of MPTP-PD model because many researchers modify their own protocols in creating MPTP-PD model.

	Acute	Sub-acute	Chronic
Dose of MPTP	20 mg/kg	30 mg/kg	30 or 45 mg/kg/day (using osmotic pump)
Duration of MPTP	3 or 4 times at 2 h interval	Once a day for 5 consecutive days	28 days
Administration of MPTP	i.p.	i.p.	i.p. (30 mg) s.c. (45 mg)
Extirpation of brain	7 days after injection	21 days after injection	28 days after pump infusion
Anticipating nigral cell loss	70%	40%	50%
Anticipating striatal fiber loss	90%	50%	50%
Notable features	Undesirable death (~10%)	Less or no undesirable death Nitrated α-synuclein accumulation	Behavioral alteration (open-field test) Formation of inclusion bodies (stained for α-synuclein, ubiquitin) Loss of noradrenergic neurons
References	[18, 19]	[18, 20]	[18, 19, 21]

nucleobases, guanine is the most susceptible to oxidation, and the C8 position of free deoxyguanosine (dG) or dGTP is the most effectively oxidized by •OH in comparison to those in DNA. In fact, eight- to nine-times more 8-oxoG is formed in nucleotide dGTP than in DNA [46, 47]. Under the oxidative stress condition, 8-oxoG accumulates in mitochondrial and nuclear DNA, which can be selectively visualized by immunohistological technique [39, 48]. Systemic MPTP administration promoted the accumulation of 8-oxoG both in mitochondria DNA and in nuclear DNA [39]. Mitochondrial 8-oxoG (mt8oxoG) accumulated in nerve terminal in the striatum, prior to nuclear 8-oxoG (nu8oxoG) accumulation in nigral dopaminergic neurons. Oka et al. [49] demonstrated that accumulation of mt8oxoG causes mitochondrial dysfunction resulting in ATP depletion, which can open the mitochondrial membrane permeability transition (MMPT) pore. During replication of mitochondrial DNA (mtDNA) with an increased level of 8-oxoG, adenine is frequently inserted opposite 8-oxoG in mtDNA, and such adenine paired with 8-oxoG is selectively excised by adenine DNA glycosylase encoded by *Mutyh* gene. During the base excision repair (BER) process, apurinic/apyrimidinic (AP) endonuclease or AP lyases convert abasic sites to single-strand breaks (SSBs) [50–53]. It has been demonstrated that the MUTYH-initiated BER causes mtDNA degradation resulting in its depletion under oxidative stress [49]. This depletion may induce a decreased supply of mitochondria-encoded proteins, transfer RNAs, and ribosomal RNAs, leading to dysfunction of mitochondrial respiration. Therefore, accumulation of mt8oxoG results in the depletion of ATP. Furthermore, MMPT opening enables Ca^{2+} to leave mitochondria, and cytoplasmic Ca^{2+} increase activates calpain, a ubiquitous calcium-sensitive protease, thus inducing cell death [49, 54]. It has been well documented that calpain activation causes the cleavage of neuronal substrates that negatively affect neuronal structure and function, leading to inhibition of essential mechanisms for neuronal survival [55]. Moreover, inhibition of calpain is known to reduce the dopaminergic neuronal loss in the MPTP model [56]. Taken together, we propose that oxidative stress in dopamine neurons initiated by MPTP administration increases accumulation of mt8oxoG, and thereby causes mitochondrial dysfunction resulting in dopaminergic neuronal loss which is dependent on the calpain pathway (Figure 1).

On the other hands, SSBs are accumulated in nuclear DNA as a result of excision of adenine opposite nu8oxoG by MUTYH, and activate poly (ADP-ribose) polymerase (PARP) with the increase of poly-ADP ribosylation, leading to nuclear translocation of apoptosis inducing factor (AIF) and NAD/ATP depletion [49]. PARP, known as a molecular nick-sensor, binds SSBs specifically and utilizes β-NAD^+ as a substrates to catalyze the synthesis of (ADP-ribose) polymers (poly-ADP ribosylation) on nuclear proteins, including PARP itself with the increase of PARP activity [57, 58]. PARP activation signal induces AIF release from mitochondria and translocation to the nucleus, which results in a caspase-independent pathway of programmed cell death [59]. Activation of PARP leads to its autoconsumption, and depletes ATP content. Therefore, a loss of energy supply also contributes to cell death [49]. Several reports indicate that PARP activation is associated with MPTP-derived neurotoxicity [60, 61]. It is, however, noteworthy that MUTYH-dependent PARP activation requires replication of nuclear DNA [49], indicating that mitotic cells in brain such as glial cells other than neurons may be affected by the PARP-AIF pathway with increased level of nu8oxoG. Among glial cells, oligodendrocytes and astrocytes show PARP-AIF pathway mediated apoptotic cell death [62, 63]. Therefore,

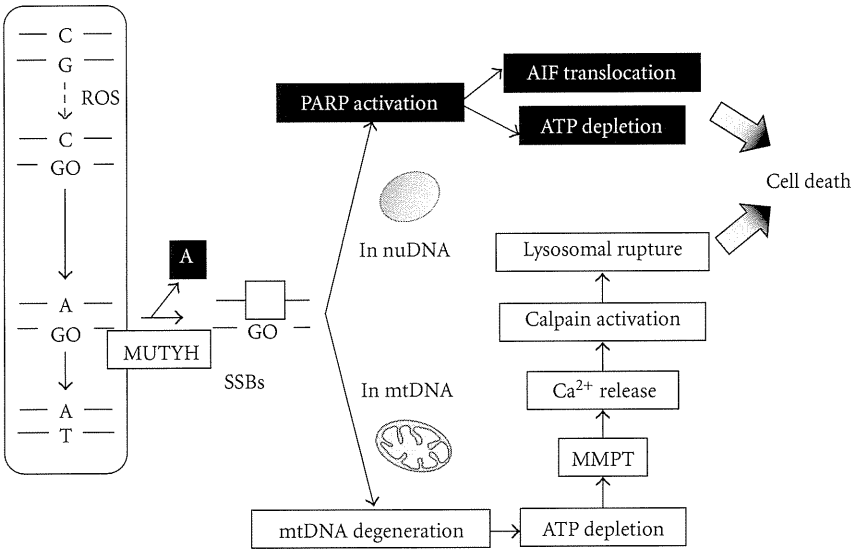

FIGURE 1: Scheme of apoptotic death signaling by accumulation of 8-oxoguanine (8-oxoG; GO) and single-strand-breaks (SSBs) in DNA. ROS, especially hydroxyl radical, increase the 8-oxoG accumulation and SSBs by MUTYH. In the case of SSBs in nucleus, activation of poly (ADP-ribose) polymerase (PARP), apoptosis inducing factor (AIF) translocation from mitochondria to nucleus, and ATP depletion followed by NAD^+ depletion leads to cellular apoptosis. On the other hands, in mitochondria, accumulation of SSBs induces mitochondrial DNA (mtDNA) degeneration. Loss of function of energy supply leads to ATP depletion, and mitochondrial membrane permeability transition (MMPT), and calpain activation results in lysosomal rupture, which potentiates cell death (modified from Figure 8, Oka et al., 2008 [49]).

accumulation of 8-oxoG in nuDNA in glial cells may thus cause caspase-independent cellular apoptosis, which might play critical roles in neurodegeneration (Figure 1).

4. 6-OHDA Model and Oxidative Damage in Nigrostriatal Neurons

For PD model animal, 6-OHDA is also used for deletion of catecholamine in the brain and in periphery [64]. 6-OHDA serves as a neurotoxin; which is readily auto-oxidized and deaminated by monoamine oxidase (MAO) [65]. Because 6-OHDA cannot penetrate blood-brain barrier, direct administration into the brain is required for the neurodegeneration in 6-OHDA model [66]. This neurotoxin can be generated within the brain by nonenzymatic reaction of dopamine, hydrogen peroxide, and free iron [67–69]. Auto-oxidation of dopamine by nitrite ions or manganese can also generate 6-OHDA [70, 71]. Oxidative damage via hydrogen peroxide and derived •OH are associated with the neurotoxic mechanism by 6-OHDA [64]. The steps to generate ROS are several varied processes: (1) in physiological condition, 6-OHDA is subjected to non-enzymatic auto-oxidation and generates several toxic products such as quinones, superoxide anion radicals, hydrogen peroxides, and •OH [65]; (2) Fenton reaction initiates and/or amplifies ROS generation. The deamination by MAO, or auto-oxidization increases the hydrogen peroxide [72, 73]. Both neurotoxins, MPTP and 6-OHDA, can potentiate the cellular apoptosis with the increase of oxidative damage in DNA, but SSBs-derived PARP activation does not affect 6-OHDA-derived cell death in embryonic nigral grafts [74]. This might be because of less formation of NO in grafted nigral neurons [75]. The apoptotic mechanism by 6-OHDA is explained by the role of p53 and Bax translocation, and caspase activation [66].

5. Hydrogen as a Therapeutic Antioxidant for Experimental Animal Models of PD

Since the first striking evidence indicating that molecular hydrogen acts as an antioxidant and inhalation of hydrogen-containing gas reduces ischemic injury in brain [76], there have been increasing reports which support therapeutic properties of hydrogen against oxidative stress-related diseases and damages in brain [77, 78], liver [79], intestinal graft [80], myocardial injury [81, 82], and atherosclerosis [83]. Hydrogen can be taken up by inhalation of hydrogen-containing gas (hydrogen gas) or drinking hydrogen-containing water (hydrogen water). One hour after the start of inhalation of hydrogen gas, hydrogen can be detectable in blood, at levels of 10 μM in arterial blood [76]. The content of hydrogen can be measured even after intake of hydrogen water by a catheter, which shows 5 μM in artery calculated after 3 min of hydrogen water incorporation [77]. Taking into account its continuous intake, it is easier and safer to drink hydrogen water than inhaling hydrogen gas.

We have previously reported that hydrogen in drinking water reduced the loss of dopaminergic neurons in MPTP-treated mice [19]. The therapeutic effects of hydrogen water against PD model have also been confirmed in another animal model, 6-OHDA-treated rats [84]. It is reported that 6-OHDA also causes 8-oxoG accumulation and mitochondrial dysfunction through oxidative stress [85], and thus our model shown in Figure 1 can be applied to the PD model.

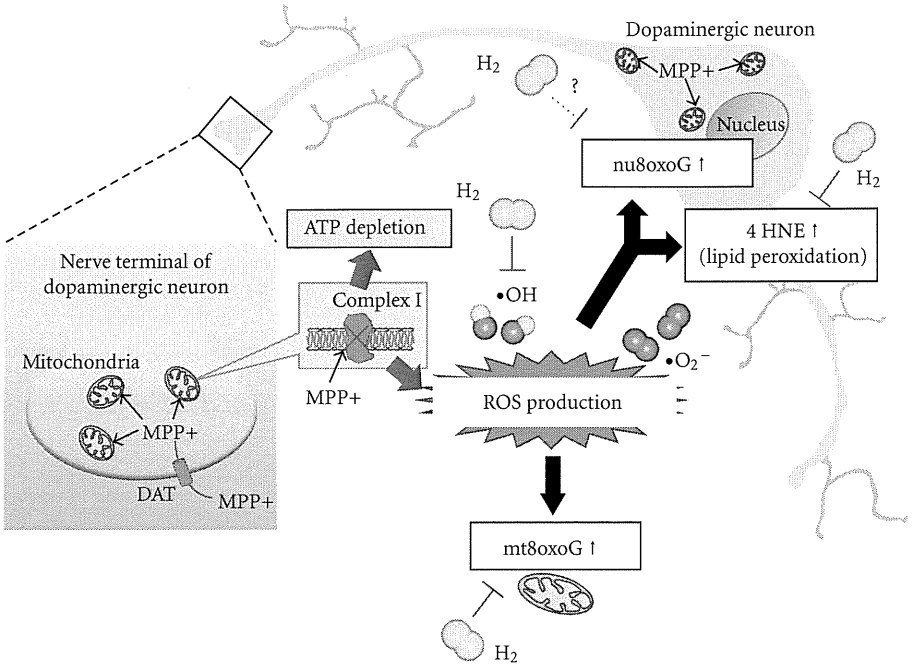

FIGURE 2: The effects of hydrogen in oxidative stress-derived neural apoptosis in dopaminergic cells. Hydrogen (H_2) selectively reduces hydroxyl radical (•OH) by direct reaction, and decreased oxidative damage such as mitochondrial/nuclear 8-oxoG (mt8oxoG/nu8oxoG) accumulation, and 4-hydroxynonenal (4-HNE) production in dopaminergic neurons. Each oxidative damage is involved in different neuronal apoptosis. Abbreviation; MPP^+: 1-methyl-4-phenylpyridinium ion, DAT: dopamine transporter, ROS: reactive oxygen species, ATP: adenosine 5′-triphosphate, •OH: hydroxyl radical, $•O_2^-$: superoxide, 4-HNE: 4-hydroxynonenal.

In these animal models, a number of dopaminergic neurons in SNpc, as well as nerve terminal fibers in striatum, were decreased by administration of the neurotoxin. However, hydrogen water significantly reduces the loss of both neuronal cell bodies and fibers compared with normal water. In MPTP-treated mice, chronic administration using an osmotic minipump results in neuronal loss as well as behavioral impairments observed by the open-field test [21]. Rats administered with 6-OHDA also show behavioral impairments assessed by the rotarod test. Hydrogen improved behavioral impairment in both MPTP and 6-OHDA model. From these observations, hydrogen water even prevents behavioral alteration which is regarded as a major symptom in PD.

It would provide us with useful information for the design of a therapeutic strategy to investigate how long the neuroprotection acquired by hydrogen water lasts. Continuous intake of hydrogen water before and during MPTP administration showed significant neuroprotection. However, intake of hydrogen water even after MPTP administration also reduced neurotoxic damage [19]. PD is regarded as a progressive neurodegenerative disease, so daily intake of hydrogen water might prevent the disease progression as well as the onset of neurodegeneration.

It has been reported that hydrogen reduced cytotoxic •OH selectively whereas the production of other radicals such as superoxide, hydrogen peroxide and nitric oxide was not altered by hydrogen [76]. This selectivity was proved by cell-free system, and in particular, the preference of scavenging of •OH rather than superoxide was confirmed in PC12 cell culture system [76]. According to Setsukinai et al. [86], both •OH and peroxynitrite ($ONOO^-$) were much more reactive than other ROS. This would be an answer why hydrogen shows selective reaction with only the strongest radicals both in the cell-free system and in PC12 cells.

Especially, •OH overproduction in oxidative and neurotoxic reaction by MPTP leads to lipid peroxidation observed by 4-hydroxynonenal (4-HNE) immunostaining in nigral dopaminergic neurons prior to cellular death. 4-HNE immunoreactivity in MPTP-treated mice is increased by three-times as much as in saline-treated mice [19], which was similar to the previous report of 4-HNE protein levels in substantia nigra observed at the same periods after MPTP administration using HPLC [41]. Hydrogen water significantly reduces the formation of 4-HNE in dopaminergic neurons in the substantia nigra to the level of control [19] (Figure 2). On the other hand, the increase of superoxide, which is detectable by administration of dihydroethidine (DHE) intravenously, was not significantly reduced by hydrogen water [19]. Although hydrogen reduces the production of superoxide in brain slices in hypoxia/reperfusion injury [87], hydrogen water might show a preferential reduction of •OH during the protection of dopaminergic neurons.

Hydrogen water significantly reduces the accumulation of 8-oxoG in striatum after MPTP administration [19] (Figure 2). As mentioned above, 8-oxoG, an oxidized form of guanine, accumulates both in mitochondria and in

nucleus; their nomenclature are mt8oxoG and nu8oxoG, respectively. Mt8oxoG accumulates in striatum which are rich in mitochondria in nerve terminal of dopaminergic neurons projected from the substantia nigra. Although nu8oxoG was not detected in nigral cell nucleus [19], hydrogen water might prevent the mt8oxoG-induced cellular apoptotic signals, not just reduce •OH in dopaminergic nerve terminals.

Hydrogen was effective when it was inhaled during reperfusion; when hydrogen was inhaled just during ischemia (not in reperfusion), infarct volume was not significantly decreased [76]. It was shown that hydrogen in the brain decreased immediately after stopping inhalation and completely disappeared within 10 min [19], indicating that the effect of hydrogen can be observed only during the period when the oxidative insults occur. Hydrogen could be detected in the blood 3 min after administration of hydrogen water into the stomach [77]. However, unpublished data showed that the half-life of hydrogen in the muscle in rats was approximately 20 min after the administration of hydrogen gas. Taking these reports into consideration, hydrogen in the brain and other tissues does not stay long enough to exert its ability as an antioxidant to ROS directly. Therefore, it is unlikely that direct reaction of hydrogen itself with ROS plays a major role in the neuroprotection, *especially by hydrogen in drinking water*, although hydrogen itself has the ability to reduce •OH preferentially. In accordance with this hypothesis, previous reports from Nakao et al. [88] has demonstrated that drinking hydrogen water increases urinary antioxidant enzyme, superoxide dismutase (SOD), an endogenous defensive system against ROS- (especially superoxide-) mediated cellular damage. Although it takes eight weeks for significant increase of SOD in humans, hydrogen has the ability to alter the expression level of urinary antioxidant enzyme. It was also reported that hydrogen water increased total bilirubin for four to eight weeks compared to baseline. Bilirubin is produced by the catalytic reaction of heme oxygenase 1 (HO-1), and degradation of heme generates bilirubin as well as carbon monoxide and free iron. The increase of HO-1 expression is likely due to the response to oxidative stress, and this response is also characterized as a phase II antioxidant which is positively regulated by several stress-responsive transcriptional factors [89]. Therefore, taking these observations into account, we might better have another aspect for protective effect of hydrogen in drinking water apart from inhalation. It is possible that drinking of hydrogen water has not only the ability to reduce cytotoxic radicals, but also novel mechanisms which are related to anti-oxidative defense system.

6. Conclusion

Oxidative stress is a key factor to induce cellular apoptosis in MPTP- and 6-OHDA-derived neurotoxicity. From studies using postmortem human brain of PD patients, increased iron, oxidation of proteins and DNA, lipid peroxidation in the SN appear to be important findings of oxidative stress [90–93]. Thought there are effective antioxidants or therapeutic strategies for PD, reduction of oxidative stress would be more desirable to attenuate neurotoxic damage in PD. Here, we would like to address that one of the most efficient ways to attenuate oxidative stress is taking low concentration of hydrogen in drinking water, a safer and easier way of hydrogen intake. Although the precise mechanism how hydrogen works is still under investigation, it will be possible to reveal the mechanisms using conventional PD models such as MPTP and 6-OHDA models. Not only that it is of great interest to know the neuroprotective mechanism of hydrogen but also hydrogen will bring great beneficial effects to reduce a risk of lifestyle-related oxidative damage and related neurodegenerative diseases including PD.

Acknowledgment

The authors thank Professor David. A. Brown (UCL, UK) for reading the paper and providing useful comments.

References

[1] W. Dauer and S. Przedborski, "Parkinson's disease: mechanisms and models," *Neuron*, vol. 39, no. 6, pp. 889–909, 2003.

[2] C. K. Glass, K. Saijo, B. Winner, M. C. Marchetto, and F. H. Gage, "Mechanisms Underlying Inflammation in Neurodegeneration," *Cell*, vol. 140, no. 6, pp. 918–934, 2010.

[3] A. E. Lang and A. M. Lozano, "Parkinson's disease," *The New England Journal of Medicine*, vol. 339, no. 15, pp. 1044–1053, 1998.

[4] A. Ziering, L. Berger, S. D. Heineman, and J. Lee, "Piperidine derivatives. Part III. 4-arylpiperidines," *Journal of Organic Chemistry*, vol. 12, no. 6, pp. 894–903, 1947.

[5] S. Przedborski, K. Tieu, C. Perier, and M. Vila, "MPTP as a mitochondrial neurotoxic model of Parkinson's disease," *Journal of Bioenergetics and Biomembranes*, vol. 36, no. 4, pp. 375–379, 2004.

[6] F. Blandini, M. T. Armentero, and E. Martignoni, "The 6-hydroxydopamine model: news from the past," *Parkinsonism and Related Disorders*, vol. 14, no. 2, pp. S124–S129, 2008.

[7] J. W. Langston, I. Irwin, E. B. Langston, and L. S. Forno, "1-Methyl-4-phenylpyridinium ion (MPP): identification of a metabolite of MPTP, a toxin selective to the substantia nigra," *Neuroscience Letters*, vol. 48, no. 1, pp. 87–92, 1984.

[8] K. Chiba, A. Trevor, and N. Castagnoli, "Metabolism of the neurotoxic tertiary amine, MPTP, by brain monoamine oxidase," *Biochemical and Biophysical Research Communications*, vol. 120, no. 2, pp. 574–578, 1984.

[9] K. Chiba, L. A. Peterson, and K. P. Castagnoli, "Studies on the molecular mechanism of bioactivation of the selective nigrostriatal toxin 1-methyl-4-phenyl-1,2,3,6-tetrahydropyridine," *Drug Metabolism and Disposition*, vol. 13, no. 3, pp. 342–347, 1985.

[10] L. A. Peterson, P. S. Caldera, A. Trevor, K. Chiba, and N. Castagnoli, "Studies on the 1-methyl-4-phenyl-2,3-dihydropyridinium Species 2,3-MPDP+, the monoamine oxidase catalyzed oxidation product of the nigrostriatal toxin 1-methyl-4-phenyl-1,2,3,6-tetrahydropyridine (MPTP)," *Journal of Medicinal Chemistry*, vol. 28, no. 10, pp. 1432–1436, 1985.

[11] J. A. Javitch, R. J. D'Amato, S. M. Strittmatter, and S. H. Snyder, "Parkinsonism-inducing neurotoxin, N-methyl-4-phenyl-1,2,3,6-tetrahydropyridine: uptake of the metabolite N-methyl-4-phenylpyridine by dopamine neurons explains

selective toxicity," *Proceedings of the National Academy of Sciences of the United States of America*, vol. 82, no. 7, pp. 2173–2177, 1985.

[12] R. R. Ramsay, J. Dadgar, A. Trevor, and T. P. Singer, "Energy-driven uptake of N-methyl-4-phenylpyridine by brain mitochondria mediates the neurotoxicity of MPTP," *Life Sciences*, vol. 39, no. 7, pp. 581–588, 1986.

[13] R. R. Ramsay and T. P. Singer, "Energy-dependent uptake of N-methyl-4-phenylpyridinium, the neurotoxic metabolite of 1-methyl-4-phenyl-1,2,3,6-tetrahydropyridine, by mitochondria," *The Journal of Biological Chemistry*, vol. 261, no. 17, pp. 7585–7587, 1986.

[14] W. J. Nicklas, I. Vyas, and R. E. Heikkila, "Inhibition of NADH-linked oxidation in brain mitochondria by 1-methyl-4-phenyl-pyridine, a metabolite of the neurotoxin, 1-methyl-4-phenyl-1,2,5,6-tetrahydropyridine," *Life Sciences*, vol. 36, no. 26, pp. 2503–2508, 1985.

[15] Y. Mizuno, N. Sone, and T. Saitoh, "Effects of 1-methyl-4-phenyl-1,2,3,6-tetrahydropyridine and 1-methyl-4-phenylpyridinium ion on activities of the enzymes in the electron transport system in mouse brain," *Journal of Neurochemistry*, vol. 48, no. 6, pp. 1787–1793, 1987.

[16] P. Chan, L. E. DeLanney, I. Irwin, J. W. Langston, and D. Di Monte, "Rapid ATP loss caused by 1-methyl-4-phenyl-1,2,3,6-tetrahydropyridine in mouse brain," *Journal of Neurochemistry*, vol. 57, no. 1, pp. 348–351, 1991.

[17] G. P. Davey, S. Peuchen, and J. B. Clark, "Energy thresholds in brain mitochondria: potential involvement in neurodegeneration," *The Journal of Biological Chemistry*, vol. 273, no. 21, pp. 12753–12757, 1998.

[18] V. Jackson-Lewis and S. Przedborski, "Protocol for the MPTP mouse model of Parkinson's disease," *Nature Protocols*, vol. 2, no. 1, pp. 141–151, 2007.

[19] K. Fujita, T. Seike, N. Yutsudo et al., "Hydrogen in drinking water reduces dopaminergic neuronal loss in the 1-methyl-4-phenyl-1,2,3,6-tetrahydropyridine mouse model of Parkinson's disease," *PLoS ONE*, vol. 4, no. 9, Article ID e7247, 2009.

[20] E. J. Benner, R. Banerjee, A. D. Reynolds et al., "Nitrated α-synuclein immunity accelerates degeneration of nigral dopaminergic neurons," *PLoS ONE*, vol. 3, no. 1, Article ID e1376, 2008.

[21] F. Fornai, O. M. Schlüter, P. Lenzi et al., "Parkinson-like syndrome induced by continuous MPTP infusion: convergent roles of the ubiquitin-proteasome system and α-synuclein," *Proceedings of the National Academy of Sciences of the United States of America*, vol. 102, no. 9, pp. 3413–3418, 2005.

[22] D. D. Song and S. N. Haber, "Striatal responses to partial dopaminergic lesion: evidence for compensatory sprouting," *Journal of Neuroscience*, vol. 20, no. 13, pp. 5102–5114, 2000.

[23] X. Du, N. D. Stull, and L. Iacovitti, "Brain-derived neurotrophic factor works coordinately with partner molecules to initiate tyrosine hydroxylase expression in striatal neurons," *Brain Research*, vol. 680, no. 1-2, pp. 229–233, 1995.

[24] J. T. Greenamyre, "Dopaminergic neurons intrinsic to the primate striatum," *Journal of Neuroscience*, vol. 17, no. 17, pp. 6761–6768, 1997.

[25] G. E. Meredith, "Immunocytochemical characterization of catecholaminergic neurons in the rat striatum following dopamine-depleting lesions," *European Journal of Neuroscience*, vol. 11, no. 10, pp. 3585–3596, 1999.

[26] M. R. Marien, F. C. Colpaert, and A. C. Rosenquist, "Noradrenergic mechanisms in neurodegenerative diseases: a theory," *Brain Research Reviews*, vol. 45, no. 1, pp. 38–78, 2004.

[27] K. S. Rommelfanger, G. L. Edwards, K. G. Freeman, L. C. Liles, G. W. Miller, and D. Weinshenker, "Norepinephrine loss produces more profound motor deficits than MPTP treatment in mice," *Proceedings of the National Academy of Sciences of the United States of America*, vol. 104, no. 34, pp. 13804–13809, 2007.

[28] E. Hasegawa, K. Takeshige, T. Oishi, Y. Murai, and S. Minakami, "1-Methyl-4-phenylpyridinium (MPP) induces NADH-dependent superoxide formation and enhances NADH-dependent lipid peroxidation in bovine heart submitochondrial particles," *Biochemical and Biophysical Research Communications*, vol. 170, no. 3, pp. 1049–1055, 1990.

[29] E. Fahre, J. Monserrat, A. Herrero, G. Barja, and M. L. Leret, "Effect of MPTP on brain mitochondrial HO and ATP production and on dopamine and DOPAC in the striatum," *Journal of Physiology and Biochemistry*, vol. 55, no. 4, pp. 325–332, 1999.

[30] T. P. Singer, R. R. Ramsay, K. McKeown, A. Trevor, and N. E. Castagnoli, "Mechanism of the neurotoxicity of 1-methyl-4-phenylpyridinium (MPP), the toxic bioactivation product of 1-methyl-4-phenyl-1,2,3,6-tetrahydropyridine (MPTP)," *Toxicology*, vol. 49, no. 1, pp. 17–23, 1988.

[31] J. M. C. Gutteridge, "Iron and oxygen radicals in brain," *Annals of Neurology*, vol. 32, pp. S16–S21, 1992.

[32] Z. I. Alam, A. Jenner, S. E. Daniel et al., "Oxidative DNA damage in the Parkinsonian brain: an apparent selective increase in 8-hydroxyguanine levels in substantia nigra," *Journal of Neurochemistry*, vol. 69, no. 3, pp. 1196–1203, 1997.

[33] J. Zhang, G. Perry, M. A. Smith et al., "Parkinson's disease is associated with oxidative damage to cytoplasmic DNA and RNA in substantia nigra neurons," *American Journal of Pathology*, vol. 154, no. 5, pp. 1423–1429, 1999.

[34] E. C. Hirsch and S. Hunot, "Neuroinflammation in Parkinson's disease: a target for neuroprotection?" *The Lancet Neurology*, vol. 8, no. 4, pp. 382–397, 2009.

[35] D. G. Graham, "Oxidative pathways for catecholamines in the genesis of neuromelanin and cytotoxic quinones," *Molecular Pharmacology*, vol. 14, no. 4, pp. 633–643, 1978.

[36] J. Boada, B. Cutillas, T. Roig, J. Bermúdez, and S. Ambrosio, "MPP^+-induced mitochondrial dysfunction is potentiated by dopamine," *Biochemical and Biophysical Research Communications*, vol. 268, no. 3, pp. 916–920, 2000.

[37] B. Drukarch and F. L. van Muiswinkel, "Neuroprotection for Parkinson's disease: a new approach for a new millennium," *Expert Opinion on Investigational Drugs*, vol. 10, no. 10, pp. 1855–1868, 2001.

[38] B. S. Mandavilli, S. F. Ali, and B. Van Houten, "DNA damage in brain mitochondria caused by aging and MPTP treatment," *Brain Research*, vol. 885, no. 1, pp. 45–52, 2000.

[39] H. Yamaguchi, K. Kajitani, Y. Dan et al., "MTH1, an oxidized purine nucleoside triphosphatase, protects the dopamine neurons from oxidative damage in nucleic acids caused by 1-methyl-4-phenyl-1,2,3,6-tetrahydropyridine," *Cell Death and Differentiation*, vol. 13, no. 4, pp. 551–563, 2006.

[40] M. L. Selley, "(E)-4-Hydroxy-2-nonenal may be involved in the pathogenesis of Parkinson's disease," *Free Radical Biology and Medicine*, vol. 25, no. 2, pp. 169–174, 1998.

[41] L. I. P. Liang, J. Huang, R. Fulton, B. J. Day, and M. Patel, "An orally active catalytic metalloporphyrin protects against 1-methyl-4-phenyl-1,2,3,6-tetrahydropyridine neurotoxicity in vivo," *Journal of Neuroscience*, vol. 27, no. 16, pp. 4326–4333, 2007.

[42] M. S. Saporito, B. A. Thomas, and R. W. Scott, "MPTP activates c-Jun NH-terminal kinase (JNK) and its upstream regulatory kinase MKK4 in nigrostriatal neurons in vivo," *Journal of Neurochemistry*, vol. 75, no. 3, pp. 1200–1208, 2000.

[43] S. Karunakaran, U. Saeed, M. Mishra et al., "Selective activation of p38 mitogen-activated protein kinase in dopaminergic neurons of substantia nigra leads to nuclear translocation of p53 in 1-methyl-4-phenyl-1,2,3,6-tetrahydropyridine-treated mice," *Journal of Neuroscience*, vol. 28, no. 47, pp. 12500–12509, 2008.

[44] S. Karunakaran and V. Ravindranath, "Activation of p38 MAPK in the substantia nigra leads to nuclear translocation of NF-κB in MPTP-treated mice: implication in Parkinson's disease," *Journal of Neurochemistry*, vol. 109, no. 6, pp. 1791–1799, 2009.

[45] M. Vila, V. Jackson-Lewis, S. Vukosavic et al., "Bax ablation prevents dopaminergic neurodegeneration in the 1-methyl-4-phenyl-1,2,3,6-tetrahydropyridine mouse model of Parkinson's disease," *Proceedings of the National Academy of Sciences of the United States of America*, vol. 98, no. 5, pp. 2837–2842, 2001.

[46] H. Kamiya and H. Kasai, "Formation of 2-hydroxydeoxyadenosine triphosphate, an oxidatively damaged nucleotide, and its incorporation by DNA polymerases. Steady-state kinetics of the incorporation," *The Journal of Biological Chemistry*, vol. 270, no. 33, pp. 19446–19450, 1995.

[47] Y. Nakabeppu, D. Tsuchimoto, H. Yamaguchi, and K. Sakumi, "Oxidative damage in nucleic acids and Parkinson's disease," *Journal of Neuroscience Research*, vol. 85, no. 5, pp. 919–934, 2007.

[48] M. Ohno, S. Oka, and Y. Nakabeppu, "Quantitative analysis of oxidized guanine, 8-oxoguanine, in mitochondrial DNA by immunofluorescence method," *Methods in Molecular Biology*, vol. 554, pp. 199–212, 2009.

[49] S. Oka, M. Ohno, D. Tsuchimoto, K. Sakumi, M. Furuichi, and Y. Nakabeppu, "Two distinct pathways of cell death triggered by oxidative damage to nuclear and mitochondrial DNAs," *The EMBO Journal*, vol. 27, no. 2, pp. 421–432, 2008.

[50] M. L. Michaels, J. Tchou, A. P. Grollman, and J. H. Miller, "A repair system for 8-oxo-7,8-dihydrodeoxyguanine," *Biochemistry*, vol. 31, no. 45, pp. 10964–10968, 1992.

[51] S. Hirano, Y. Tominaga, A. Ichinoe et al., "Mutator phenotype of MUTYH-null mouse embryonic stem cells," *The Journal of Biological Chemistry*, vol. 278, no. 40, pp. 38121–38124, 2003.

[52] Y. Tominaga, Y. Ushijima, D. Tsuchimoto et al., "MUTYH prevents OGG1 or APEX1 from inappropriately processing its substrate or reaction product with its C-terminal domain," *Nucleic Acids Research*, vol. 32, no. 10, pp. 3198–3211, 2004.

[53] M. L. Michaels, J. Tchou, A. P. Grollman, and J. H. Miller, "A repair system for 8-oxo-7,8-dihydrodeoxyguanine," *Biochemistry*, vol. 31, no. 45, pp. 10964–10968, 1992.

[54] G. Simbula, P. A. Glascott Jr., S. Akita, J. B. Hoek, and J. L. Farber, "Two mechanisms by which ATP depletion potentiates induction of the mitochondrial permeability transition," *American Journal of Physiology*, vol. 273, no. 2, pp. C479–C488, 1997.

[55] P. S. Vosler, C. S. Brennan, and J. Chen, "Calpain-mediated signaling mechanisms in neuronal injury and neurodegeneration," *Molecular Neurobiology*, vol. 38, no. 1, pp. 78–100, 2008.

[56] S. J. Crocker, P. D. Smith, V. Jackson-Lewis et al., "Inhibition of calpains prevents neuronal and behavioral deficits in an MPTP mouse model of Parkinson's disease," *Journal of Neuroscience*, vol. 23, no. 10, pp. 4081–4091, 2003.

[57] T. Eki and J. Hurwitz, "Influence of poly(ADP-ribose) polymerase on the enzymatic synthesis of SV40 DNA," *The Journal of Biological Chemistry*, vol. 266, no. 5, pp. 3087–3100, 1991.

[58] C. Soldani and A. I. Scovassi, "Poly(ADP-ribose) polymerase-1 cleavage during apoptosis: an update," *Apoptosis*, vol. 7, no. 4, pp. 321–328, 2002.

[59] S. W. Yu, H. Wang, M. F. Poitras et al., "Mediation of poty(ADP-ribose) polymerase-1—dependent cell death by apoptosis-inducing factor," *Science*, vol. 297, no. 5579, pp. 259–263, 2002.

[60] A. S. Mandir, S. Przedborski, V. Jackson-Lewis et al., "Poly(ADP-ribose) polymerase activation mediates 1-methyl-4-phenyl-1,2,3,6-tetrahydropyridine (MPTP)-induced parkinsonism," *Proceedings of the National Academy of Sciences of the United States of America*, vol. 96, no. 10, pp. 5774–5779, 1999.

[61] H. Wang, M. Shimoji, S. W. Yu, T. M. Dawson, and V. L. Dawson, "Apoptosis inducing factor and PARP-mediated injury in the MPTP mouse model of Parkinson's disease," *Annals of the New York Academy of Sciences*, vol. 991, pp. 132–139, 2003.

[62] S. Veto, P. Acs, J. Bauer et al., "Inhibiting poly(ADP-ribose) polymerase: a potential therapy against oligodendrocyte death," *Brain*, vol. 133, no. 3, pp. 822–834, 2010.

[63] C. C. Alano, W. Ying, and R. A. Swanson, "Poly(ADP-ribose) polymerase-1-mediated cell death in astrocytes requires NAD depletion and mitochondrial permeability transition," *The Journal of Biological Chemistry*, vol. 279, no. 18, pp. 18895–18902, 2004.

[64] R. Heikkila and G. Cohen, "Inhibition of biogenic amine uptake by hydrogen peroxide: a mechanism for toxic effects of 6-hydroxydopamine," *Science*, vol. 172, no. 3989, pp. 1257–1258, 1971.

[65] G. Cohen and R. E. Heikkila, "The generation of hydrogen peroxide, superoxide radical, and hydroxyl radical by 6 hydroxydopamine, dialuric acid, and related cytotoxic agents," *The Journal of Biological Chemistry*, vol. 249, no. 8, pp. 2447–2452, 1974.

[66] D. Blum, S. Torch, N. Lambeng et al., "Molecular pathways involved in the neurotoxicity of 6-OHDA, dopamine and MPTP: contribution to the apoptotic theory in Parkinson's disease," *Progress in Neurobiology*, vol. 65, no. 2, pp. 135–172, 2001.

[67] A. Slivka and G. Cohen, "Hydroxyl radical attack on dopamine," *The Journal of Biological Chemistry*, vol. 260, no. 29, pp. 15466–15472, 1985.

[68] K. Jellinger, L. Linert, E. Kienzl, E. Herlinger, and M. B. H. Youdim, "Chemical evidence for 6-hydroxydopamine to be an endogenous toxic factor in the pathogenesis of Parkinson's disease," *Journal of Neural Transmission, Supplement*, no. 46, pp. 297–314, 1995.

[69] W. Linert, E. Herlinger, R. F. Jameson, E. Kienzl, K. Jellinger, and M. B. H. Youdim, "Dopamine, 6-hydroxydopamine, iron, and dioxygen—their mutual interactions and possible implication in the development of Parkinson's disease," *Biochimica et Biophysica Acta*, vol. 1316, no. 3, pp. 160–168, 1996.

[70] A. Palumbo, A. Napolitano, P. Barone, and M. D'Ischia, "Nitrite- and peroxide-dependent oxidation pathways of dopamine: 6- nitrodopamine and 6-hydroxydopamine formation as potential contributory mechanisms of oxidative stress- and nitric oxide-induced neurotoxicity in neuronal degeneration," *Chemical Research in Toxicology*, vol. 12, no. 12, pp. 1213–1222, 1999.

[71] C. D. Garner and J. P. Nachtman, "Manganese catalyzed auto-oxidation of dopamine to 6-hydroxydopamine in vitro," *Chemico-Biological Interactions*, vol. 69, no. 4, pp. 345–351, 1989.

[72] G. R. Breese and T. D. Traylor, "Depletion of brain noradrenaline and dopamine by 6-hydroxydopamine," *British Journal of Pharmacology*, vol. 42, no. 1, pp. 88–99, 1971.

[73] F. Karoum, S. J. Chrapusta, M. F. Egan, and R. J. Wyatt, "Absence of 6-hydroxydopamine in the rat brain after treatment with stimulants and other dopaminergic agents: a mass fragmentographic study," *Journal of Neurochemistry*, vol. 61, no. 4, pp. 1369–1375, 1993.

[74] G. S. Kaminski Schierle, O. Hansson, E. Ferrando-May, P. Nicotera, P. Brundin, and M. Leist, "Neuronal death in nigral grafts in the absence of poly (ADP-ribose) polymerase activation," *NeuroReport*, vol. 10, no. 16, pp. 3347–3351, 1999.

[75] F. L. van Muiswinkel, B. Drukarch, H. W. M. Steinbusch, and J. De Vente, "Sustained pharmacological inhibition of nitric oxide synthase does not affect the survival of intrastriatal rat fetal mesencephalic transplants," *Brain Research*, vol. 792, no. 1, pp. 48–58, 1998.

[76] I. Ohsawa, M. Ishikawa, K. Takahashi et al., "Hydrogen acts as a therapeutic antioxidant by selectively reducing cytotoxic oxygen radicals," *Nature Medicine*, vol. 13, no. 6, pp. 688–694, 2007.

[77] K. Nagata, N. Nakashima-Kamimura, T. Mikami, I. Ohsawa, and S. Ohta, "Consumption of molecular hydrogen prevents the stress-induced impairments in hippocampus-dependent learning tasks during chronic physical restraint in mice," *Neuropsychopharmacology*, vol. 34, no. 2, pp. 501–508, 2009.

[78] Y. Gu, C. S. Huang, T. Inoue et al., "Drinking hydrogen water ameliorated cognitive impairment in senescence-accelerated mice," *Journal of Clinical Biochemistry and Nutrition*, vol. 46, no. 3, pp. 269–276, 2010.

[79] K. I. Fukuda, S. Asoh, M. Ishikawa, Y. Yamamoto, I. Ohsawa, and S. Ohta, "Inhalation of hydrogen gas suppresses hepatic injury caused by ischemia/reperfusion through reducing oxidative stress," *Biochemical and Biophysical Research Communications*, vol. 361, no. 3, pp. 670–674, 2007.

[80] B. M. Buchholz, D. J. Kaczorowski, R. Sugimoto et al., "Hydrogen inhalation ameliorates oxidative stress in transplantation induced intestinal graft injury," *American Journal of Transplantation*, vol. 8, no. 10, pp. 2015–2024, 2008.

[81] A. Nakao, D. J. Kaczorowski, Y. Wang et al., "Amelioration of rat cardiac cold ischemia/reperfusion injury with inhaled hydrogen or carbon monoxide, or both," *Journal of Heart and Lung Transplantation*, vol. 29, no. 5, pp. 544–553, 2010.

[82] K. Hayashida, M. Sano, I. Ohsawa et al., "Inhalation of hydrogen gas reduces infarct size in the rat model of myocardial ischemia-reperfusion injury," *Biochemical and Biophysical Research Communications*, vol. 373, no. 1, pp. 30–35, 2008.

[83] I. Ohsawa, K. Nishimaki, K. Yamagata, M. Ishikawa, and S. Ohta, "Consumption of hydrogen water prevents atherosclerosis in apolipoprotein E knockout mice," *Biochemical and Biophysical Research Communications*, vol. 377, no. 4, pp. 1195–1198, 2008.

[84] Y. Fu, M. Ito, Y. Fujita et al., "Molecular hydrogen is protective against 6-hydroxydopamine-induced nigrostriatal degeneration in a rat model of Parkinson's disease," *Neuroscience Letters*, vol. 453, no. 2, pp. 81–85, 2009.

[85] E. C. Stack, J. L. Ferro, J. Kim et al., "Therapeutic attenuation of mitochondrial dysfunction and oxidative stress in neurotoxin models of Parkinson's disease," *Biochimica et Biophysica Acta*, vol. 1782, no. 3, pp. 151–162, 2008.

[86] K. I. Setsukinai, Y. Urano, K. Kakinuma, H. J. Majima, and T. Nagano, "Development of novel fluorescence probes that can reliably detect reactive oxygen species and distinguish specific species," *The Journal of Biological Chemistry*, vol. 278, no. 5, pp. 3170–3175, 2003.

[87] Y. Sato, S. Kajiyama, A. Amano et al., "Hydrogen-rich pure water prevents superoxide formation in brain slices of vitamin C-depleted SMP30/GNL knockout mice," *Biochemical and Biophysical Research Communications*, vol. 375, no. 3, pp. 346–350, 2008.

[88] A. Nakao, Y. Toyoda, P. Sharma, M. Evans, and N. Guthrie, "Effectiveness of hydrogen rich water on antioxidant status of subjects with potential metabolic syndrome—an open label pilot study," *Journal of Clinical Biochemistry and Nutrition*, vol. 46, no. 2, pp. 140–149, 2010.

[89] J. Alam and J. L. Cook, "How many transcription factors does it take to turn on the heme oxygenase-1 gene?" *American Journal of Respiratory Cell and Molecular Biology*, vol. 36, no. 2, pp. 166–174, 2007.

[90] D. T. Dexter, F. R. Wells, F. Agid et al., "Increased nigral iron content in postmortem Parkinsonian brain," *The Lancet*, vol. 2, no. 8569, pp. 1219–1220, 1987.

[91] A. Yoritaka, N. Hattori, K. Uchida, M. Tanaka, E. R. Stadtman, and Y. Mizuno, "Immunohistochemical detection of 4-hydroxynonenal protein adducts in Parkinson disease," *Proceedings of the National Academy of Sciences of the United States of America*, vol. 93, no. 7, pp. 2696–2701, 1996.

[92] Z. I. Alam, S. E. Daniel, A. J. Lees, D. C. Marsden, P. Jenner, and B. Halliwell, "A generalised increase in protein carbonyls in the brain in Parkinson's but not incidental Lewy body disease," *Journal of Neurochemistry*, vol. 69, no. 3, pp. 1326–1329, 1997.

[93] H. Shimura-Miura, N. Hattori, D. Kang, K. I. Miyako, Y. Nakabeppu, and Y. Mizuno, "Increased 8-oxo-dGTPase in the mitochondria of substantia nigral neurons in Parkinson's disease," *Annals of Neurology*, vol. 46, no. 6, pp. 920–924, 1999.

Published OnlineFirst April 5, 2011; DOI:10.1158/0008-5472.CAN-10-3482

Molecular and Cellular Pathobiology

Cancer Research

Frequent Truncating Mutation of *TFAM* Induces Mitochondrial DNA Depletion and Apoptotic Resistance in Microsatellite-Unstable Colorectal Cancer

Jianhui Guo[1], Li Zheng[2,3], Wenyong Liu[2,4], Xianshu Wang[2], Zemin Wang[1], Zehua Wang[1], Amy J. French[2], Dongchon Kang[5], Lin Chen[6], Stephen N. Thibodeau[2], and Wanguo Liu[1]

Abstract

The mitochondrial transcription factor A (TFAM) is required for mitochondrial DNA (mtDNA) replication and transcription. Disruption of TFAM results in heart failure and premature aging in mice. But very little is known about the role of TFAM in cancer development. Here, we report the identification of frequent frameshift mutations in the coding mononucleotide repeat of *TFAM* in sporadic colorectal cancer (CRC) cell lines and in primary tumors with microsatellite instability (MSI), but not in microsatellite stable (MSS) CRC cell lines and tumors. The presence of the *TFAM* truncating mutation, in CRC cells with MSI, reduced the TFAM protein level *in vivo* and *in vitro* and correlated with mtDNA depletion. Furthermore, forced overexpression of wild-type TFAM in RKO cells carrying a *TFAM* truncating mutation suppressed cell proliferation and inhibited RKO cell-induced xenograft tumor growth. Moreover, these cells showed more susceptibility to cisplatin-induced apoptosis due to an increase of cytochrome *b* (Cyt *b*) expression and its release from mitochondria. An interaction assay between TFAM and the heavy-strand promoter (HSP) of mitochondria revealed that mutant TFAM exhibited reduced binding to HSP, leading to reduction in Cyt *b* transcription. Collectively, these data provide evidence that a high incidence of *TFAM* truncating mutations leads to mitochondrial copy number reduction and mitochondrial instability, distinguishing most CRC with MSI from MSS CRC. These mutations may play an important role in tumorigenesis and cisplatin-induced apoptotic resistance of most microsatellite-unstable CRCs. *Cancer Res; 71(8); 2978–87. ©2011 AACR.*

Introduction

Colorectal cancers (CRC) display 2 major types of genomic instability: chromosomal instability (CIN) and microsatellite instability (MIN or MSI; 1). CRC exhibiting MSI is characterized by the inactivation of DNA mismatch repair (MMR) proteins (2). As a consequence, tumors with MSI accumulate genetic alterations in both coding and noncoding microsatellite repeats, which are widely distributed throughout the genome (1, 3). MSI occurs in ~90% of cancers in patients with hereditary nonpolyposis CRC and in 10% to 15% of sporadic CRC (4). Since the inactivation of an MMR gene by itself is unlikely to result in a transforming event, additional genetic changes are believed to be required for cells to become malignant. In addition to the large number of microsatellite repeat alterations in noncoding regions that have been reported in CRC with MSI, many genes with frameshift mutations in their coding repeats have also been documented. Examples include *TGFBRII*, *BAX*, *AXIN2*, and *HDAC2* (5–9). Functional analyses of some of these mutants have demonstrated that frameshift mutations can lead to loss of tumor suppressor function and are probably responsible for driving tumorigenesis in colonic tissues (6, 9). Therefore, it is critical to identify the genes carrying frameshift mutations in their coding repeats and defining their roles in tumorigenesis for an improved understanding of the etiology of CRC with MSI. Furthermore, this will provide valuable information for prognostic evaluation and better therapeutic intervention.

On screening for potential mutation targets of deficient MMR, we identified a coding poly(A)$_{10}$ repeat in the *TFAM* gene. TFAM (also known as mtTF1, mtTFA, or TCF6) is a mitochondrial transcription factor (10). It regulates mtDNA transcription and replication, and plays a critical role in maintaining mtDNA copy number and mitochondrial morphology (10–12). *Tfam* heterozygous knockout mice exhibited

Authors' Affiliations: [1]Department of Genetics, Louisiana State University Health Sciences Center, New Orleans, Louisiana; [2]Department of Laboratory Medicine & Pathology, Mayo Clinic, Rochester, Minnesota; [3]Department of Pathology, Jiaotong University; [4]Department of Surgery, Ninth People's Hospital, Shanghai, China; [5]Department of Clinical Chemistry and Laboratory Medicine, Kyushu University, Fukuoka, Japan; and [6]Life Technologies, Carlsbad, California

Note: Supplementary data for this article are available at Cancer Research Online (http://cancerres.aacrjournals.org/).

Jianhui Guo, Li Zheng, and Wenyong Liu contributed equally to this work.

Corresponding Author: Wanguo Liu, Department of Genetics, Louisiana State University Health Sciences Center, New Orleans, LA 70112. Phone: 504-568-5143; Fax: 504-568-8500; E-mail: wliu2@lsuhsc.edu

doi: 10.1158/0008-5472.CAN-10-3482

Published OnlineFirst April 5, 2011; DOI:10.1158/0008-5472.CAN-10-3482

a 50% reduction in both *Tfam* transcription and Tfam protein levels, resulting in a marked reduction in the mtDNA copy number (11). TFAM and mtDNA copy number have been shown to be critical for the regulation of mitochondrial gene expression; their reduction leads to reduced heart function and aging (13, 14). Moreover, the depletion of mtDNA and reduction of TFAM-dependent mtDNA expression are involved in infantile mitochondrial myopathy, Alzheimer disease, and Parkinson disease (13, 15, 16).

In the present study, we explored the role of TFAM in colorectal carcinogenesis. We identified a high frequency of *TFAM* truncating mutations, showed low level of TFAM protein and reduced mtDNA copy number in both CRC cell lines and primary CRC tissues with MSI. We also examined the effect of the mutant TFAM on tumorigenesis, mitochondrial gene expression, and cisplatin-induced apoptotic resistance. Our results indicate that *TFAM* mutations induce mtDNA depletion and result in decreased tumor sensitivity to cisplatin in most CRC with MSI. The presence of these alterations suggests the potential importance of TFAM in tumorigenesis of CRC with MSI and implicates TFAM-dependent mitochondrial instability as a unique pathogenetic factor for CRC with MSI. *TFAM* mutation may be potentially useful in predicting outcomes and selecting chemotherapy for patients with microsatellite-unstable CRC.

Materials and Methods

Tumor tissues and cell lines

Eighty-nine CRC tissue specimens including 43 MSI and 46 MSS collected at Mayo Clinic were previously described (6). Seventeen CRC cell lines including 11 with MSI (LS174T, Co115, LoVo, TC7, HCT-15, HCT 116, TC71, SW48, RKO, HCT-8, and LS411) and 6 MSS (SW480, SW837, COLO205, SW620, HT-29, and Caco-2), as well as 4 endometrial cancer cell lines with MSI (HEC-1-A, HEC59, Ishika14, and RL95–2), 1 gastric cancer cell line with MSI (SNU-1), and 4 non-CRC cell lines (LNCaP, SKBR3, MDA-MB231, and MCF-7) were obtained from American Type Culture Collection. Cells were cultured in medium by the standard protocol. Genomic DNA from tissues or cell lines was isolated using Easy-DNA Kit (Invitrogen) following the manufacturer's instructions.

Mutation analysis

PCR was performed using the forward primer in exon 4 of *TFAM*: 5′-ATAAAGAAGAGATAAGCAGATT-3′ and the reverse primer in intron 5: 5′-TGCCTATTAAGAGAAAACTAC-3′ following the condition previously described (17). Mutations were determined by direct sequencing analyses of the PCR products (18). All mutations were confirmed by repeated PCR amplification and bidirectional sequencing analysis.

Western blotting

The whole cell lysates, cytosol, and mitochondria fractions were isolated from cells as previously described (19). Western blot analysis was performed following the protocol described before (17) using rabbit polyclonal TFAM antibody (20) and antibodies against Cyt *b*, cleaved PARP-1, and cleaved Casp-3 (Cell Signaling), β-actin and β-tubulin, and the corresponding HRP-conjugated secondary antibodies (Sigma), respectively.

Immunofluorescence and immunohistochemistry analyses

For immunofluorescence analysis, cells grown on the 12-well chamber slides were incubated with 100 nmol/L MitoTracker Red CMVRos (Invitrogen) for 20 minutes. Cells were then washed, fixed, and blocked in 1% bovine serum albumin–PBS, incubated with primary antibodies and goat antirabbit secondary antibody conjugated to Alexa 488 (Invitrogen). Microscopy was performed on LSM510 Carl Ziess Confocal Laser Scanning Microscope. For immunohistochemical analysis, tissue sections were deparaffinized, rehydrated, and treated in 3% H_2O_2–methanol to remove endogenous peroxidase. The sections were then boiled in 10 mmol/L citric acid buffer (pH 6.0) for 20 minutes for antigen retrieval, followed by incubation with anti-TFAM antibody (20), biotinylated goat antisera, and streptavidin peroxidase (Jackson ImmunoResearch). Detection was done using 3,3′-diaminobenzidine (Vector Labs). Sections were scored as 0 (−, negative), 1 (+, weak positive), 2 (++, medium positive), and 3 (+++, strong positive), respectively.

Determination of mtDNA copy number and mitochondrial mass

The mtDNA copy number was determined by quantitative real time PCR (qPCR) using the Platinum SYBR Green qPCR SuperMix-UDG with ROX (Invitrogen) on ABI PRISM 7900 Sequence Detector (Applied Biosystems; 21). The primer sequences used were ND1-F1, 5′-CACCCAAGAACAGGGTTTGT-3′ and ND1-R1, 5′-TGGCCATGGGATTGTTGTTAA-3′ for mitochondrial NADH dehydrogenase 1 (*ND1*), and β-actin-F, 5′-TCCCAGCACACTTAACTTAGC-3′ and β-actin-R, 5′-AGCCACAAGAAACACTCAGG-3′, for β-*actin* (nuclear DNA control), respectively. Relative copy number was calculated from the threshold cycle value (Ct value) using the delta delta Ct (ΔΔCT) method (22). Each reaction was optimized and confirmed to be linear within an appropriate concentration range using genomic DNA from a normal colon epithelial cell line CRL1807. The mitochondrial mass was determined using flow cytometry. Briefly, 1×10^6 cells were labeled with 100 nmol/L MitoTracker Red CMXRos (M7512, Invitrogen) in Dulbecco's modified Eagle medium containing 10% FBS and incubated at 37°C for 30 minutes, washed and resuspended in 1 mL PBS with 1% FBS. Individual cellular fluorescence signals were analyzed compared to unstained cells as controls using FACSCalibur and CellQuest Pro software (BD Biosciences).

RNA extraction and qRT-PCR

Total RNA was extracted using Trizol reagent (Invitrogen) following the manufacturer's instructions. The first strand cDNA was synthesized by Superscript III First-Strand Kit (Invitrogen). qRT-PCR was carried out with ABI Prism 7900 using primers: ND1-F2, 5′-TCGCCCTATTCTTCATAGCC-3′ and ND1-R2, 5′-AGAAGTAGGGTCTTGGTGAC-3′ for *ND1*; CYTB-F, 5′-CTATCCATCCTCATCCTAGC-3′ and CYTB-R,

Published OnlineFirst April 5, 2011; DOI:10.1158/0008-5472.CAN-10-3482

5′-TGGTTGTCCTCCGATTCAGG-3′ for mitochondrial cytochrome *b* gene (*CYTB*), respectively. Glyceraldehyde-3-phosphate dehydrogenase (*GAPDH*) was used as an internal control with primers GAPDH-F, 5′-TCCCAGCACACTTAACTTAGC-3′ and GAPDH-R, 5′-AGCCACAAGAAACACTCAGG-3′. Relative expression levels of *ND1* and *CYTB* were calculated by the ΔΔCT method as described above.

Constructs, lentivirus preparation, and infection

The full-length wild-type TFAM (Wt-TFAM) cDNA was PCR-amplified and cloned into pCMV-tag5b expression vector (Strategene). The mutant TFAM (Mut-TFAM) was created using the pCMV-tag5b-Wt-TFAM as a template by deleting 1 A in the poly(A)$_{10}$ region using QuickChange XL site-directed mutagenesis kit (Stratagene) following the supplier's instructions. Lentiviral constructs expressing Wt- or Mut-TFAM were generated by inserting the PCR products of the full-length Wt- or Mut-TFAM-Myc gene into pCDH-CMV-MCS-EF1-copGFP vector (System Biosciences) with the *Bam*H1/*Not*I restriction sites, respectively. To express the GST (glutathione S transferase) fusion proteins of mature Wt- or Mut-TFAM in *Escherichia coli*, the Wt- or Mut-TFAM without the mitochondrial target sequence (1–43 amino acid residues) was amplified by PCR using pCMV-tag5b-Wt- or Mut-TFAM-Myc as templates and cloned into pGEX-4T-1 vector (GE Healthcare) with *Bam*H1/*Not*I restriction sites. All constructs were verified by sequencing and immunoblotting. Lentivirus production and cell infection were performed according to the manufacturer's instructions.

Separation and analyses of mitochondrial NP-40-soluble and -insoluble fractions

Mitochondrial NP-40-soluble and -insoluble fractions were separated and analyzed as previously described (23) with modification. Briefly, mitochondria (1.0 mg protein/mL) isolated from RKO cells expressing Wt-TFAM-Myc, Mut-TFAM-Myc, or control vector were resuspended in TES buffer (10 mmol/L Tris–HCl, pH 7.4, 0.25 mol/L sucrose, 1 mmol/L EDTA) containing 1× protease inhibitor mix and 0.5% NP-40. After incubation (30 minutes on ice) and centrifugation (20,000 × *g*, 30 minutes, 4°C), samples were separated into a pellet (P1) and a supernatant (S1). The P1 fractions were resuspended in mitochondrial lysis buffer, centrifuged (20,000 × *g*, 30 minutes) and supernatants (S2) were collected. Equal volumes of S1 or S2 fractions were subjected to 15% SDS-PAGE and detected by immunoblotting using anti-TFAM antibody. In addition, the mtDNA in P1 and S1 fractions were extracted (23) and subjected to PCR amplification and gel electrophoresis analysis.

Interaction assay of TFAM protein with mitochondrial heavy-strand promoter

GST-Wt-TFAM and GST-Mut-TFAM fusion proteins were generated as previously described (20) and purified using BugBuster GST Bind Purification Kit following manufacturer's instruction (Novagen). The mitochondrial heavy-strand promoter (HSP) was generated by annealing 2 complementary oligonucleotides HSP-F: 5′-CACACACCGCTGCTAACCC-CATACCCCGAACCAACCAAACCCCAAAGACACCCCC-3′ and HSP-R: 5′-GGGGGTGTCTTTGGGGTTTGGTTGGTTCGGGG-TATGGGGTTAGCAGCGGTGTGTG-3′. The interaction assay was performed as previously described (24) with modification. Briefly, the reactions were performed in 50 μL binding buffer (20 mmol/L HEPES pH 7.6, 100 mmol/L NaCl, 1 mmol/L EDTA, 0.1% NP40) containing 500 nmol/L HSP and 0, 20, 50, 100, 200, or 400 nmol/L of GST, GST-Wt-TFAM or GST-Mut-TFAM proteins. After incubation with glutathione-sepharose beads and centrifugation, the supernatants containing the unbound HSP were subjected to qPCR analysis using primers corresponding to the mitochondrial HSP, hsp-rtF: 5′-CACACACCGCTGCTAAC-3′ and hsp-rtR: 5′-GGGTGTCTTTGGGGTTT-3′. The levels of protein-bound HSP were determined by subtracting the unbound HSP.

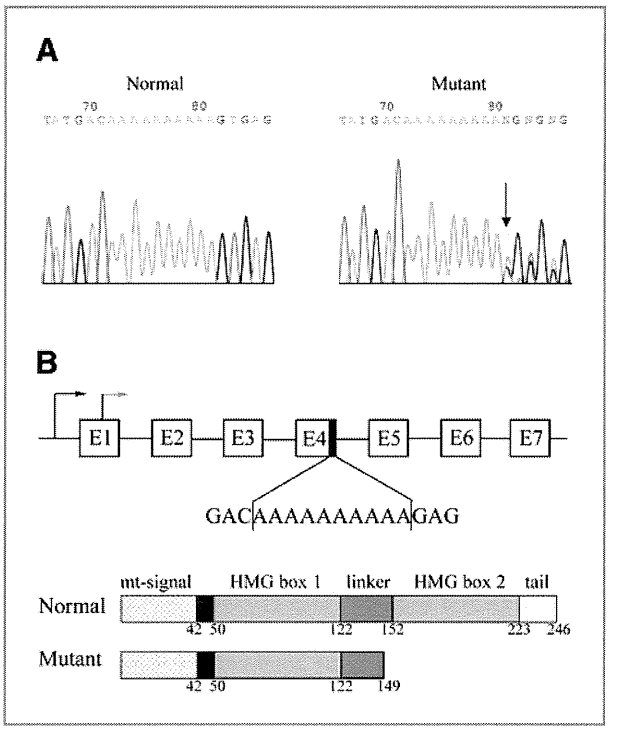

Figure 1. Sequence analysis of *TFAM* frameshift mutation in human CRC. A, sequence chromatograms of *TFAM* poly(A)$_{10}$ mononucleotide repeat in normal (left) and CRC tissue (right). Arrow indicates the mutation site. B, genomic and domain structures of human TFAM. Frameshift *TFAM* mutation in the poly(A)$_{10}$ mononucleotide repeat region of exon 4 results in a truncated protein lacking the C-terminus of TFAM, including a small portion of the linker domain, the entire HMG box2 domain, and the tail domain.

Cell proliferation and apoptosis assays

For cell proliferation assay, cells infected with Lenti-vector, -Wt-TFAM, or -Mut-TFAM were seeded in 6-well plates (0.3 × 10^5 cells/well in triplicate) and counted daily for 5 days using a hemacytometer with trypan blue staining. For apoptosis analysis, the infected cells were treated with cisplatin (50 μmol/L/mL, 12 hours), followed by propidium iodide staining

Published OnlineFirst April 5, 2011; DOI:10.1158/0008-5472.CAN-10-3482

Table 1. *TFAM* mutations identified in cancer cell lines with or without MSI

Tumor cell lines	MS status	Cell line	A_{10} allele status
Colorectal cancer			
	MSI	Co115	A9/A10
	MSI	LS174T	A9/A10
	MSI	LoVo	A9/A10
	MSI	TC71	A9/A10
	MSI	HCT15	A9/A10
	MSI	HCT116	A9/A10
	MSI	TC7	A9/A10
	MSI	SW48	A9/A10
	MSI	RKO	A8/A10
	MSI	HCT8	A9/A10
	MSI	LS411	A9/A10
	MSS	SW480	A10
	MSS	SW837	A10
	MSS	Colo205	A10
	MSS	SW620	A10
	MSS	HT-29	A10
	MSS	Caco-2	A10
Endometrial cancer			
	MSI	HEC-1A	A9/A10
	MSI	HEC59	A9/A10
	MSI	Ishika14	A9/A10
	MSI	RL95-2	A10
Gastric cancer			
	MSI	SNU-1	A9/A10

(25) and analyzed by the FACScan flow cytometer (Coulter Epics XL-MSL, Beckman Coulter).

Xenograft tumor growth assay

Cells infected with various lentiviral constructs grown to 70% to 80% confluences in complete medium were harvested with trypsin–EDTA and washed with PBS. Cells were counted and suspended in sterile PBS at a concentration of 2.0×10^7 cells/mL. Five-week-old nude mice (NCI) were inoculated s.c. in the left and right hind flanks with 200 μL cell suspension. Tumor development was closely monitored and pictures of mice were taken 3 weeks after inoculation.

Statistical analysis

Data are presented as mean ± SE. Student's *t* test was used to compare means of 2 independent groups. One-way ANOVA and post hoc Turkey's test was applied to analyze the difference of means of more than 2 groups. A $P < 0.05$ was considered statistically significant using SigmaStat 3.5 (Systat Software).

Results

TFAM frameshift mutations in primary CRCs and cell lines

We analyzed the poly$(A)_{10}$ mononucleotide repeat within exon 4 of the *TFAM* gene for mutations in 17 CRCs cell lines and 89 CRC tissue specimens. We detected a mutation frequency of 100% (11/11) in CRC cell lines and 74.4% (32/43) in CRC tissue specimens with MSI. All the mutations displayed a heterozygous deletion of 1 base in the mononucleotide A track, except 1 cell line and 4 tissue specimens that displayed a 2-base deletion (Fig. 1A and Table 1). The *TFAM* frameshift mutation was also detected in 3 of 4 endometrial and 1 gastric cancer cell lines with MSI but not in 6 CRC cell lines and 46 CRC tissue specimens without MSI, nor in DNA isolated from normal individuals and cancer cell lines without MSI (Table 1 and data not shown). These data clearly demonstrate that the frequent frameshift mutation of the *TFAM* gene is unique to microsatellite-unstable cancers, particularly to microsatellite-unstable CRC, distinguishing them from MSS CRC.

TFAM mutation results in reduction in TFAM protein level

The *TFAM* frameshift mutation is predicted to result in a protein truncation at codon 149 (Leu149Stop; Δ149), leading to the deletion of the entire region of the second HMG domain and the tail region (Fig. 1B). To assess the putative effect of the mutation, we analyzed TFAM levels in 10 CRC cell lines (5 with MSI and 5 without MSI) by Western blotting using the TFAM polyclonal antibody. All 5 CRC cell lines with MSI showed reduced TFAM protein levels as compared to those in the 5 MSS CRC cell lines (Fig. 2A). Similar results were obtained by another TFAM antibody (ABCOM, Ab 47517, data not shown).

Published OnlineFirst April 5, 2011; DOI:10.1158/0008-5472.CAN-10-3482

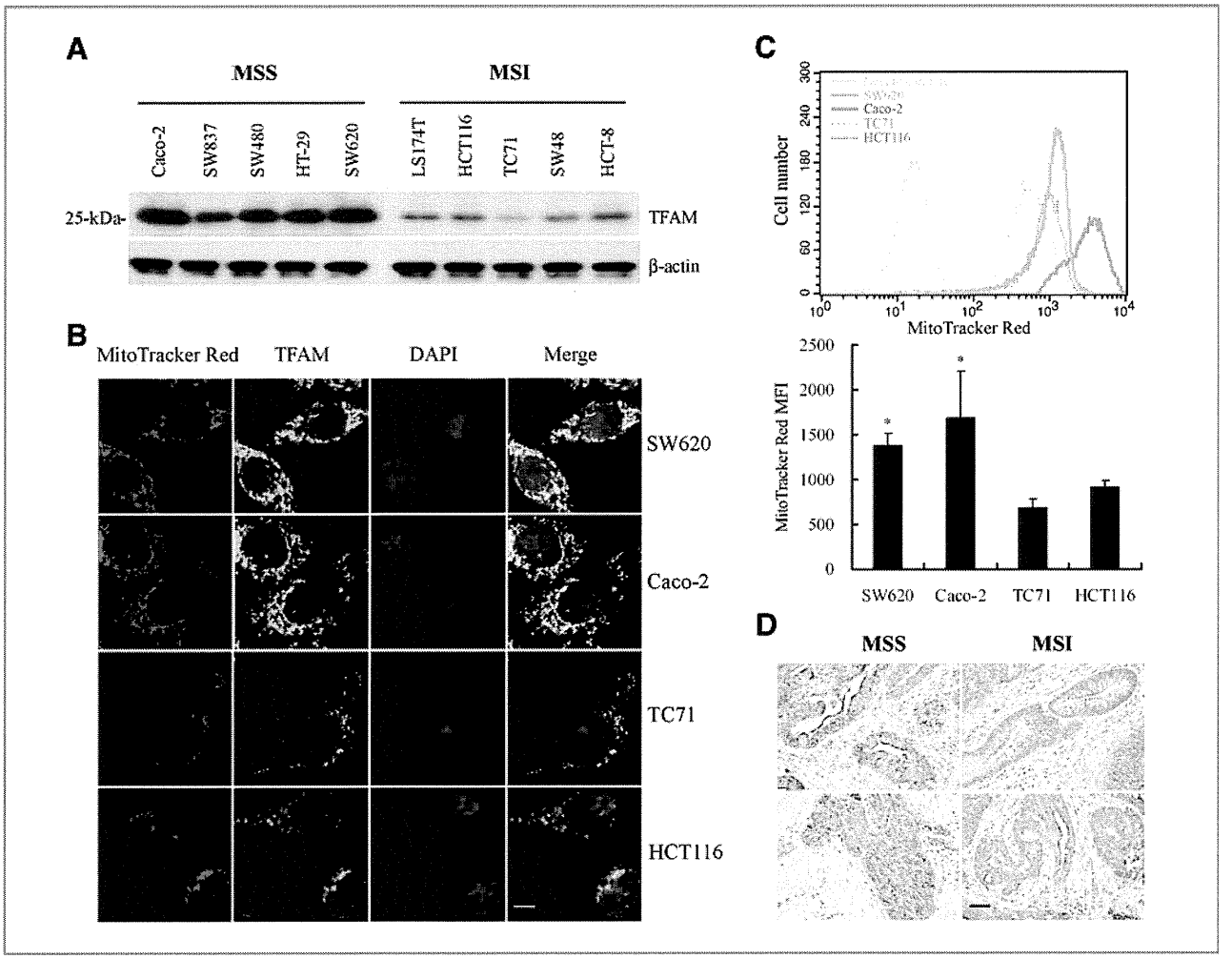

Figure 2. *TFAM* frameshift mutation results in reduction of TFAM protein and mtDNA in CRC with MSI. A, relatively low levels of TFAM protein in CRC cell lines with MSI and *TFAM* mutations compared to those in MSS CRC cell lines. B, immunofluorescent analysis of TFAM (green) and mitochondria (red) in MSS CRC cells (Caco2 and SW837) and CRC cells with MSI (HCT116 and TC71). Scale bar indicates 10 μm. C, mitochondrial mass of CRC cells. Shown here are flow cytometry curves for cells as in (B; top), and average values of the mean fluorescent intensity (MFI) of MitoTracker Red (bottom, $P < 0.05$). Results represent mean ± SE of 3 independent experiments. D, representative images of TFAM immunohistochemical analysis in 2 CRC specimens with MSI carrying *TFAM* mutations and 2 MSS CRC specimens. Positive TFAM immunoreactivity appeared brown in cytoplasm. Scale bar indicates 50 μm.

In agreement with the Western blot data, immunofluorescence analysis showed relatively lower levels of TFAM protein in CRC cells with MSI than in MSS CRC cells (Fig. 2B). In addition, cells with reduced TFAM expression exhibited reduced mitochondrial mass compared to that in MSS CRC cell lines shown by decreased MitoTracker labeling (Fig. 2B and C). To examine the above observations *in vivo*, we performed immunohistochemical analysis of TFAM in 20 primary CRC specimens. Nine of the 10 CRC with MSI carrying *TFAM* mutations showed low levels of TFAM, while all 7 CRC with MSI carrying no *TFAM* mutations and 3 MSS CRC specimens displayed strong levels of TFAM (Fig. 2D). Taken together, these *in vitro* and *in vivo* data suggest that the *TFAM* truncating mutation correlates with the reduction in TFAM protein in most CRC with MSI.

TFAM mutation leads to mtDNA depletion in CRC

Reduction in TFAM protein has been shown to induce mtDNA depletion in *Tfam* knockout mice and in cultured mammalian cells (11, 26). To determine whether this is also the case in CRC with MSI, we performed qPCR of mtDNA from 17 CRC cell lines, using the *ND1* gene as the mtDNA marker and β-actin as a nuclear control. We first determined the efficiency and reproducibility of the method using a normal colon epithelial cell line (CRL-1807) as a control and generated a standard curve (Supplementary Fig. S1). The results indicated that the mtDNA copy number in 11 CRC cell lines with MSI was significantly lower than that in the 6 MSS CRC cell lines (1:2.63, $P < 0.01$; Fig. 3A, left). Similar results were obtained on analysis of 4 non-CRC cell lines with MSI (Table 1) and 5 non-CRC cell lines (LNCaP, SKBR3, RL95-2,

Published OnlineFirst April 5, 2011; DOI:10.1158/0008-5472.CAN-10-3482

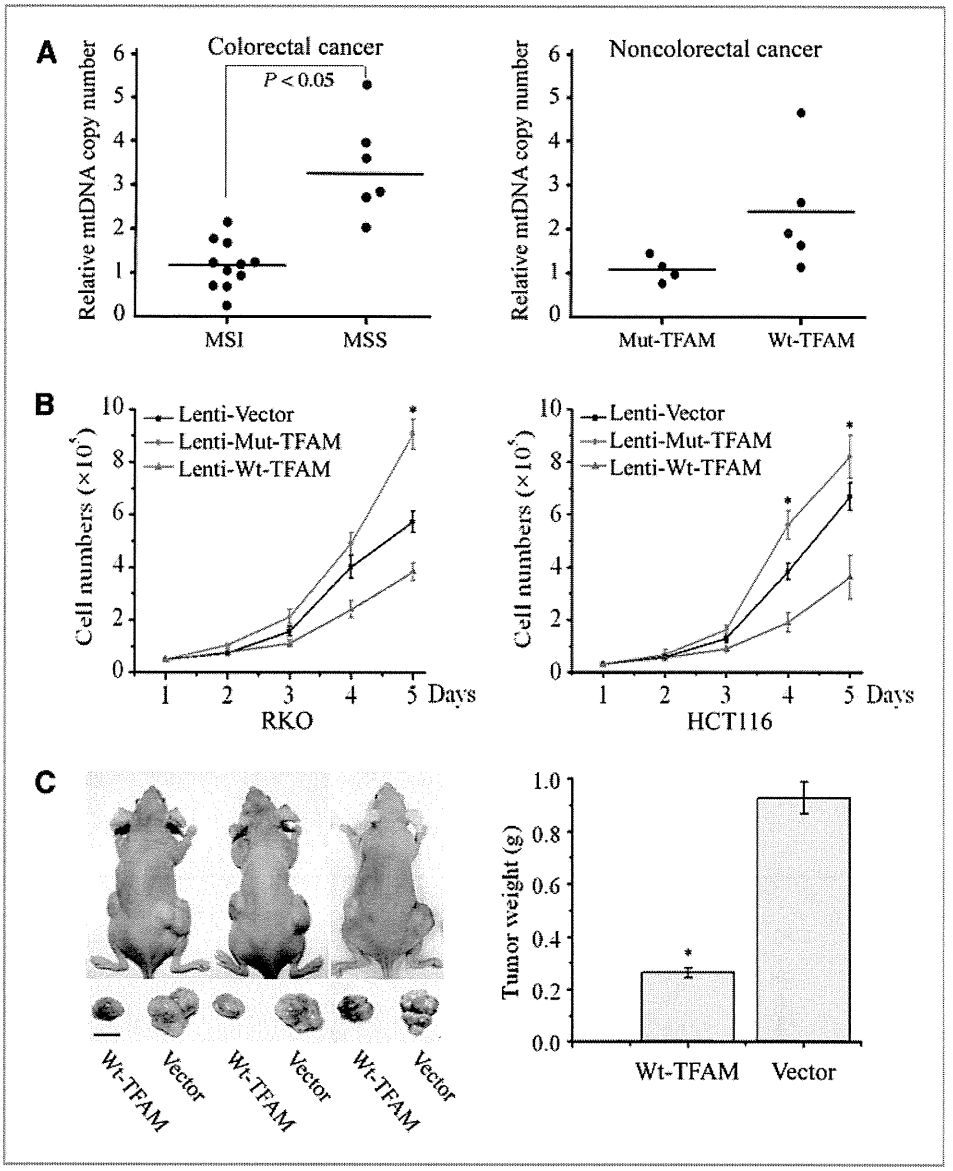

Figure 3. Effects of mutant TFAM on mtDNA depletion and tumor cell growth. A, mtDNA copy number of CRC (left) and non-CRC cells (right) by qPCR analysis. Each dot represents the mean value of 3 independent measurements of each genomic DNA sample. Solid horizontal lines represent the mean value of each dataset. B, cell proliferation curves of RKO (left) and HCT116 cells (right). Data represent mean ± SE of 3 independent experiments in triplicates, $P < 0.05$ for all. C, representative photograph showing the difference of tumor size in nude mice injected with Wt-TFAM- or vector-expressing RKO cells (left, scale bar indicates 5 mm). The averaged tumor weights were significantly different (right, $P < 0.01$). Values represent mean ± SE of tumors from 5 pairs of mice.

MDA-MB231, and MCF-7), which do not carry *TFAM* mutations (Fig. 3A, right). These data demonstrate that the *TFAM* truncating mutation resulting in TFAM protein reduction led to the decrease in mtDNA copy number in CRC with MSI.

Mut-TFAM promotes tumorigenesis in CRC

To assess the potential role of the mut-TFAM in CRC tumorigenesis, we performed a cell proliferation assay using the RKO CRC cell line, which harbors a *TFAM* truncating mutation. The growth rates of RKO cells infected with Lenti-Mut-TFAM or Lenti-Wt-TFAM were compared with the growth rates of RKO cells infected with Lenti-vector. The expression level of exogenous TFAM (Wt- or Mut-TFAM) was about 10% of the level of endogenous TFAM and appeared no apparent toxic effect on cells compared to the cells infected with Lenti-vector (Supplementary Fig. S2A and B). We found that the cells expressing Mut-TFAM grew faster, while the cells expressing Wt-TFAM grew slower than the control cells ($P < 0.05$, Fig. 3B, left). Similar results were observed in the HCT116 CRC cell line, which also harbors a *TFAM* truncating mutation (Fig. 3B, right). To determine the cell growth suppression potential of Wt-TFAM *in vivo*, we implanted athymic nude mice with RKO cells expressing the Lenti-vector or Lenti-Wt-TFAM on the right or left hind flank, respectively. Consistent with the *in vitro* cell proliferation data, RKO cells infected with Wt-TFAM induced much smaller tumors than those induced by the control RKO cells (Fig. 3C, left). The weight of the tumors induced by Wt-TFAM was reduced by more than 70% compared to those induced by control RKO cells ($P < 0.01$, Fig. 3C, right). These results suggest that the *TFAM* truncating